UNIVERSITY OF CALIFORNIA SAN DIEGO

Transport of Indirect Excitons in GaAs Heterostructures

A dissertation submitted in partial satisfaction of the
requirements for the degree
Doctor of Philosophy

in

Physics

by

Matthew William Hasling

Committee in charge:

Professor Leonid Butov, Chair
Professor Shaya Fainman
Professor Misha Fogler
Professor Yu-Hwa Lo
Professor Congjun Wu

2018

The dissertation of Matthew William Hasling is approved, and it is acceptable in quality and form for publication on microfilm and electronically:

_____

_____

_____

_____

_____

Chair

University of California San Diego

2018

DEDICATION

To my wife, Anna, who has been the greatest support anyone could ever ask for.

EPIGRAPH

You're only given a little spark of madness.

You mustn't lose it.

—Robin Williams

TABLE OF CONTENTS

LIST OF FIGURES

ACKNOWLEDGEMENTS

I would like to begin this section by thanking my advisor, Professor Leonid Butov. None of the work presented here would have been possible without his constant guidance and support. He has made sure that I stayed focused on the pursuit of academic knowledge, and has always been an amazing source of information and ideas.

Without the help of Chelsey Dorow and Erica Calman, I never would have gotten this far. I would like to thank both of them for supporting me throughout graduate school. We fought through a great deal together, and they have both kept my spirits and curiosity alive, even in the toughest times.

One of the greatest sources of motivation for me throughout grad school has been my family. Mom, Dad, Mike, Ashley, thank you for always being there to convince me to follow through with my dreams.

I would also like to thank Brad Hanson, Sharmila Poddar, and Tom Murphy, who have always known that I could finish this, even when I wasn't sure myself.

Most of all, I would like to thank my wife Anna, who has been the pinnacle of support and love through all of the difficulties that this process has presented. I would not be the person I am today without you, and I never would have made it this far without you.

The text of chapter 3, in part, is a reprint of the material as it appears in Y.Y. Kuznetsova, P. Andreakou, M.W. Hasling, J.R. Leonard, E.V. Calman, L.V. Butov, M. Hanson, A.C. Gossard, Two-dimensional snowflake trap for indirect excitons, *Optics Letters*, 40, 589, 2015. The co-authors in this publication directed, supervised, and co-worked on the research which forms the basis of this chapter.

The text of chapter 3, in part, is a reprint of the material as it appears in M.W. Hasling, Y.Y. Kuznetsova, P. Andreakou, J.R. Leonard, E.V. Calman, C.J. Dorow, L.V. Butov, M. Hanson, A.C. Gossard, Stirring potential for indirect excitons, *Journal of Applied Physics*, 117, 023108, 2015, where the dissertation author was the first author. The co-authors in this publication directed,

supervised, and co-worked on the research which forms the basis of this chapter.

VITA

2012	B. A. in Physics, Pomona College
2012-2014	Graduate Teaching Assistant, University of California San Diego
2017	Instructor, University of California San Diego

PUBLICATIONS

C. J. Dorow, M. W. Hasling, E. V. Calman, L. V. Butov, J. Wilkes, K. L. Campman, and A. C. Gossard, "Spatially and time-resolved imaging of transport of indirect excitons in high magnetic fields", *Phys. Rev. B*, 95, 235308 2017.

Y.Y. Kuznetsova, P. Andreakou, M.W. Hasling, J.R. Leonard, E.V. Calman, L.V. Butov, M. Hanson, A.C. Gossard, "Two-dimensional snowflake trap for indirect excitons", *Optics Letters*, 40, 589, 2015.

M.W. Hasling, Y.Y. Kuznetsova, P. Andreakou, J.R. Leonard, E.V. Calman, C.J. Dorow, L.V. Butov, M. Hanson, A.C. Gossard, "Stirring potential for indirect excitons", *Journal of Applied Physics*, 117, 023108, 2015.

ABSTRACT OF THE DISSERTATION

Transport of Indirect Excitons in GaAs Heterostructures

by

Matthew William Hasling

Doctor of Philosophy in Physics

University of California San Diego, 2018

Professor Leonid Butov, Chair

Indirect excitons are bosonic quasiparticles composed of an electron and a hole confined to spatially separated quantum wells. Many properties of excitons, such as their low effective mass, long lifetime, tunable energy, and optically active nature, make them an ideal system for studying condensed matter phenomena. This dissertation explores the transport properties associated with indirect excitons in various environments.

In this dissertation, exciton transport is studied in multiple devices, created by carefully patterned electrodes, which create a varied potential energy landscape for the excitons. The first device is used to trap large amounts of excitons, which can be used to study the properties of dense exciton gases. The second device is used as a stirring potential for indirect excitons, and

can give excitons angular momentum while they collect to the center of the device. In addition, a record high quality single quantum well structure is characterized, which may prove to be a new platform for studying indirect excitons. Measurements of this new sample show large transport and a record high diffusion coefficient for indirect excitons.

Chapter 1

Introduction

1.1 Introduction to Excitons

When an incoming photon interacts with a semiconductor, it can excite an electron from the valence band into the conduction band. When this happens, a hole is also generated in the semiconductor. When these two particles bind together to form one particle, it is known as an exciton. Since an exciton is one particle composed of two spin-1/2 particles, it is a boson. Bosons exhibit many interesting properties, including the ability to form bosonic condensates. Countless studies of bosonic particles and the condensates they form have been conducted over the years, many of which were performed with atomic bosons. Excitons have a significantly smaller mass than atomic bosons, and can be studied in different regimes. For instance, the high magnetic field regime for atomic bosons is in the range of 10^6 T, which is well outside the range of what can be achieved in a cryostat like ours. For excitons, the high magnetic field regime can be reached with just a few Tesla.

Since an exciton is composed of an electron and a hole, the two particles that compose an exciton will recombine and emit a photon. Studying the emission position and energy of the emitted photons is the main way we study the properties of excitons.

1.2 Indirect Excitons

The excitons that we primarily study are known as indirect excitons (IX), or more specifically, spatially indirect excitons. The samples that were used in this work contain two spatially separated quantum wells that the electron and hole of the exciton can occupy while maintaining the bond that makes them an exciton. An electric field can then be applied to the sample, causing the electron to occupy one well with the hole in the other well, as shown in Figure 1.1. Keeping the electron and hole spatially separated provides multiple advantages, including a long and controllable lifetime, increased transport distances, disorder screening, and the ability to control the excitons through applied voltage.

1.2.1 Long and controllable lifetime

Keeping the electron and hole spatially separated suppresses the overlap of the electron and hole wavefunctions. Therefore, there is a lower probability of recombination, and radiative recombination is suppressed. This results in lifetimes orders of magnitude higher than lifetimes of direct excitons. This lifetime can be affected by different CQW structures and by the strength

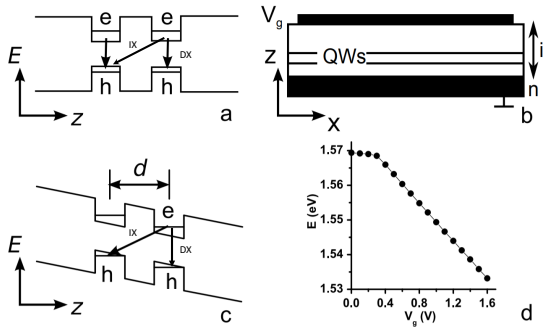

Figure 1.1: Sample diagrams and IX schematic: (a) Band diagram in a CQW structure with zero bias. (b) Positioning the CQW between a ground electrode and an electrode at voltage Vg creates an electric field in the z-direction and (c) moves the electrons and holes in opposite directions and thus different quantum wells. (d) Exciton energy E as a function of Vg. At low voltages, direct excitons are energetically favorable, and Vg has nearly no effect on E. At sufficiently high voltages, the energy of indirect excitons decreases, and indirect excitons become the ground state. Their energy varies linearly with the electric field and thus Vg.

of the applied electric field [4].

1.2.2 Control by Voltage

Since an indirect exciton is an electric dipole, the energy of indirect excitons is controllable by the applied voltage, as seen in Figure 1.1d [15, 11]. Thus, creating a varying landscape of electric fields in a sample creates an energy landscape for the excitons and can influence the motion of the excitons.

1.2.3 Disorder Screening

As previously stated, indirect excitons are electric dipoles, and the applied electric field causes them to be aligned dipoles with dipole moment ed, where d is the separation between the QW centers. These aligned dipoles have a repulsive force between them, due to the dipole-dipole interaction. This repulsive force allows them to screen in-plane disorder in the structure [24].

1.2.4 Increased Transport Distances

Due to the long lifetimes of indirect excitons and the disorder screening caused by the dipole-dipole interaction, indirect excitons can travel long distances before decaying. These transport distances can be as high as tens or hundreds of micrometers [15, 5, 31]. These transport distances are long enough to accommodate lithography of electrode patterns that create the potential landscapes previously discussed.

1.2.5 Cooling

Excitons generated by laser excitation are initially at high temperatures, but due to the long transport distances and long lifetimes of excitons, they are able to cool to the lattice temperature

of the material they exist in [6]. Samples in our cryostats can reach lattice temperatures of as low as 30mK.

1.3 Pattern Formation

Because of the long lifetime and long transport distances of indirect excitons in CQW structures, the luminescence pattern of indirect excitons can take various forms. One such pattern is the inner ring structure, which is caused by the fact that the excitons at the excitation spot are at a high temperature, but cool as they move away from the excitation spot [29]. A significant percentage of the excitons at the excitation spot occupy high energy states that are not optically active, and as they move away from the laser spot, they relax into low energy, optically active states. This leads to a decrease in photoluminescence at the excitation spot, and the peak of the photoluminescence exists at some distance from the laser excitation, causing a ring shape when the excitation is at a point. Other patterns observed in indirect exciton studies include the external ring, localized bright spots, and macroscopically ordered exciton states [7].

1.4 Devices

The energy of an indirect exciton is directly correlated to the applied electric field perpendicular to the plane of the sample, given by $E_{ex} = -F_z ed$. Varying this applied electric field over an in-plane (x-y) area creates a potential energy landscape for excitons. Many different types of devices have been created to explore the possibilities of the uses of indirect excitons. Devices that have been created and tested include ramps [15, 11, 10], static and moving lattices [56, 57, 16, 39, 41, 55] , traps [22, 12, 18, 48, 51, 36], and transistors [3]. One of the large focuses of this dissertation involves a device that was based off of the idea of a moving lattice, but also functions as a trap. It also works based off of the principle that increased electrode density at

the surface of a CQW structure leads to an increased electric field within the structure [28].

Chapter 2

Experimental Methods

2.1 Samples

The research discussed in chapter 3 was conducted with coupled quantum well structure (CQW), and the research discussed in chapter 5 was conducted with a wide single quantum well structure (WSQW). These samples were grown with molecular-beam epitaxy to produce the highest quality samples possible, provided by collaborating groups. When the samples are grown, the quantum wells are placed close to the back gate to minimize in-plane electric fields that could cause exciton dissociation [16]. Electrodes were then patterned onto the surface of the samples to create the desired energy landscape for the excitons. This work was done in the clean room at Nano3 at UCSD. The electrodes are composed of either Ti or ITO, depending on the sample, and are patterned onto the surface of the sample using various lithography techniques. Some are made using photolithography, but electrodes with finer features require electron beam lithography. Once the electrodes are attached, gold pads are also patterned onto the sample, allowing for electrical connections to be made to the electrodes and the back gate of the sample. The sample is then placed into a socket, fixed with melted indium, and connections are made with gold wires to connect the sample to the sample socket, where external electrical contacts can be made.

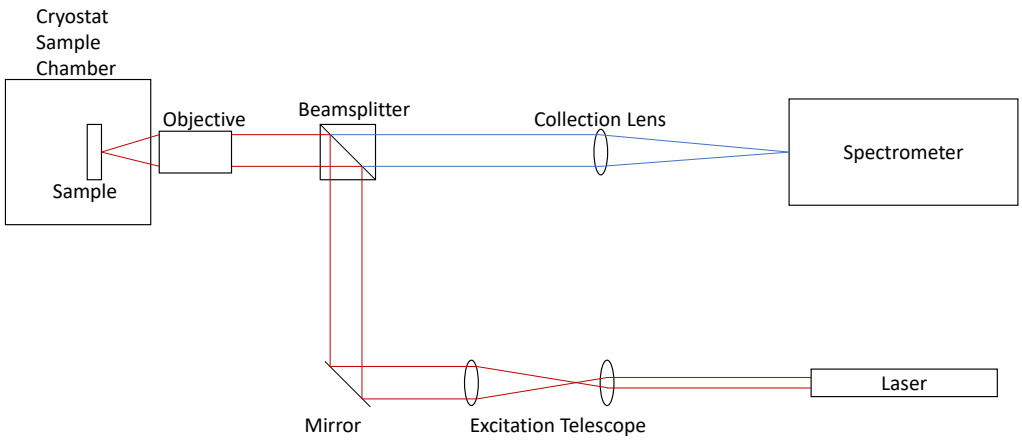

Figure 2.1: Diagram of optics in the experimental setup.

2.2 Experimental Setup

The start of the experimental setup used for these experiments is the cryostat used to bring the sample down to low temperatures. For these experiments, a cryostat from the Janis Research Company was used, and the data was taken at typical temperatures of 1.7K. A drawing of the cryostat is shown in Figure 2.2. The cryostat has an insert which allows for electrical connections to be made from an external voltage source, and windows, which allow for laser excitation and optical measurement. The laser excitation is provided by a variety of lasers, depending on various factors, including the wavelength and power required, and whether the laser required is pulsed or not. The lasers used in these experiments included helium-neon lasers, titanium-sapphire lasers, and diode lasers. As shown in Figure 2.1, an excitation telescope is then installed to focus the beam to the desired excitation profile. The laser then passes through a beamsplitter, which allows the beam to reflect towards the sample, but optical measurements can still be made through it. Then the laser passes through an objective, which in these experiments is a Mitutoyo M-Plan

APO 10x objective. The signal from the sample is then collected via a collection lens and passed to a spectrometer with a nitrogen-cooled CCD. Using this, we can observe the light from the excitons either as X-Y images or as X-Energy images, which allow for simultaneous spatial and spectral resolution.

Chapter 3

Snowflake Trap and Stirring Potential for Indirect Excitons

3.1 Snowflake Trap

Potential traps made possible the realization of cold and dense atom gases and, eventually, the achievement of atom condensation. Traps also allow control of the confined gases by in-situ varying the trap shape and depth. Similarly, potential traps are an effective tool for studying the physics of cold excitons – cold bosons in condensed matter materials.

The realization of a cold and dense exciton gas in a trap requires a long exciton lifetime, which allows excitons to travel to the trap center and cool to low temperatures before recombination. An indirect exciton in a coupled quantum well structure (CQW) is composed of an electron and a hole in spatially separated layers (Fig. 3.1a). Lifetimes of indirect excitons are orders of magnitude longer than lifetimes of regular excitons, which allows the creation of trapping potentials where the indirect excitons are optically generated over the trap area and can reach the trap center. Although indirect excitons are typically hot when generated in the region of optical excitation, their long lifetimes allow them to cool below the temperature of quantum degeneracy

a few nanoseconds after the generation [6] or a few microns away from the excitation spot [17]. Due to the small exciton mass, the temperature of quantum degeneracy for indirect excitons in GaAs CQW can be achieved at ~ 1 K, which has allowed the observation of exciton condensation and spontaneous coherence in a trap at helium refrigerator temperatures [19].

Creating electrostatic traps for excitons requires control by voltage. Indirect excitons have a built-in dipole moment ed, where d is the separation between the electron and hole layers. As a result, their energy can be controlled by voltage: an electric field F_z perpendicular to the QW plane results in the exciton energy shift $-edF_z$ [37]. This gives the opportunity to realize the desired potential landscape for indirect excitons $E(x,y) = -edF_z(x,y)$ and control it by voltage $in-situ$, on time scales shorter than the exciton lifetime. Indirect excitons were studied in various electrostatically created potential landscapes including ramps [15, 11, 34], lattices [57, 26, 40, 39], traps [22, 16, 9, 18, 21, 19, 49, 25, 47, 48, 51], and circuit devices [20, 13, 3].

Of particular interest is a trap which can provide a confining potential with the exciton energy gradually reducing towards the trap center. Such a confining potential could collect excitons from a large area, creating a dense exciton gas at the trap center. This, in turn, can facilitate the creation of a degenerate exciton gas in the trap since the temperature of quantum degeneracy is roughly proportional to the particle density. Furthermore, such potentials direct and confine excitons and, as a result, concentrate the energy transported via excitons thus operating as excitonic antennas. Directing and concentrating the energy can be explored in excitonic devices, for instance in molecular and polymeric solar cells [2].

Creating a trap with a confining in-plane potential on a large area is challenging. In this paragraph, we briefly overview the earlier studied electrostatic traps for indirect excitons. (i) A trap can be created by a circular opening in an electrode [16] or by a circular electrode [9, 51]. In these traps, the in-plane potential varies within a small length from the electrode edge $\sim D$, where D is the distance between the top and bottom electrode [21]. Since D is typically small (1 μm in our samples) these traps produce a confining in-plane potential on a small area. Large

traps of this type have a box-like shape [21]. (ii) A confining potential can be realized by laterally modulated voltage. These traps are produced by electrodes at different voltages and the exciton energy reduces from electrode to electrode towards the trap center [22, 16, 18, 49, 25, 47, 48]. The achievement of a large area of confining potentials in these traps requires a large number of separately contacted electrodes. In-plane voltage gradients in these traps may produce in-plane electric currents heating the excitons. (iii) Confining potentials for indirect excitons can be realized by using a single electrode: In earlier studies, this was achieved in the diamond-shaped traps [21]. The diamond-shaped traps offered the largest area for confining potentials studied so far. However, the elongated shape of the diamond traps limits the area of exciton collection, and as a result, limits the number of excitons collected in the trap center. In the earlier studies of exciton condensation and spontaneous coherence in the diamond trap, a total exciton number in the trap was limited [19, 35].

In this work, we present experimental proof of principle for a new electrostatic trap for indirect excitons – the snowflake trap. The advantages of snowflake traps include the ability to produce a two-dimensional confining potential for indirect excitons on a large area, an order of magnitude larger than the diamond traps, using a single electrode with no exciton heating by in-plane electric currents. The operation principle of snowflake traps is based on the control of exciton energy by electrode density. The CQW is placed between a flat ground plane and a snowflake-shaped electrode, resulting in varying F_z in the CQW plane due to fringing electric fields from a shaped electrode. Decreasing electrode density toward the trap edges reduces F_z and in turn, exciton energy shift, producing a confining potential for indirect excitons [28].

The experiments were done at 1.6 K. Excitons were photogenerated by 700 nm Ti:Sapphire laser. The emission images were taken by a nitrogen-cooled CCD camera. An interference filter selecting the spectral range of the indirect exciton emission was used for measuring $x-y$ images. A spectrometer with resolution 0.18 meV was used for measuring $x-$energy images. The spatial resolution was 1.5 μm.

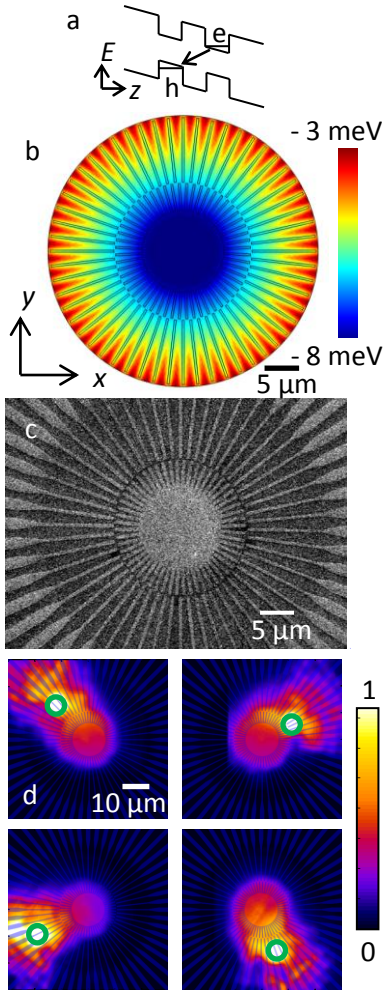

Figure 3.1: Diagrams and XY Images of Trap: a, CQW diagram. e, electron; h, hole. b, Calculated indirect exciton energy shift $E(x,y) = -edF_z(x,y)$ in the snowflake trap. Center and outer electrode voltage $V_c = V_o = -0.65$ V. c, SEM image of the electrode pattern forming the snowflake trap for indirect excitons. d, $x-y$ emission images of indirect excitons for four different positions of the laser excitation spot. The excitation spot positions are given by green circles. The circle size corresponds to the excitation spot size. For each of the images in d, the positions of the excitation spot and exciton emission cloud relative to the trap center are indicated by the overlaid electrode pattern (with the central part deleted for clarity). For all excitation spot positions, the generated excitons are effectively collected to the trap center by the trap potential. $V_c = -8$ V, $V_o = -6.5$ V, size of focused laser excitation spot $s = 7$ μm, excitation power $P \sim 50$ μW.

A snowflake trap can be created using a single snowflake-shaped electrode. However, in this work, the snowflake trap is formed by a snowflake-shaped pattern for a center electrode and

separate outer electrodes. This design was chosen to enable this device to function as a stirring potential, but this also allows us to control the shape of the confining potential by varying the voltages on the center and outer electrodes independently. The outer electrode pattern starts 10 μm from the trap center. An SEM image of the snowflake electrode pattern is presented in Fig. 3.1c. The electrode density is adjusted to create a 2D in-plane potential profile for indirect excitons with the exciton energy gradually reducing toward the trap center from any direction.

Figure 3.1b shows the simulated exciton energy in the snowflake trap for a uniform voltage applied to the center and outer electrodes ($V_c = V_o = -0.65$ V). The simulations were done using COMSOL Inc. Multiphysics software. The simulations show a confining potential in all directions with an energy minimum at the trap center.

The emission of indirect excitons for four different positions of the laser excitation spot is presented in Fig. 3.1d. The excitation spot positions are given by green circles. Figure 3.1d demonstrates the experimental proof of principle for the snowflake trap: For any position of the laser excitation spot, the generated excitons are effectively collected to the trap center by the trap potential.

Note that some excitons are also trapped towards the outside direction of the trap (Fig. 3.1d). In this "contact region" outside the snowflake trap the electrodes become thicker for better contacts, which increases the electrode density and, as a result, lowers the exciton energy causing the "outside trapping".

We also studied the effect of varying voltage and excitation power on the trap profile. Figures 3.2a-c, 3.2g-1, and 3.3a,c demonstrate control of the shape of snowflake trap by voltage. The reduction of absolute value of voltage on the center electrode V_c for fixed voltage on the outer electrode pattern V_o makes the trap shallower (Figs. 3.2a, 3.2g, and 3.3a,c). Alternatively, increasing $\mid V_c \mid$ and keeping V_o fixed makes the trap deeper and facilitates exciton collection to the trap center (Figs. 3.2c,i and 3.3a,b).

Figures 3.2d-f, 3.2j-l, and 3.3b,d show that as the density of indirect excitons increases,

so does the exciton energy in the trap, and the trap becomes shallower. Such energy variation is consistent with the screening of the trap potential by the repulsively interacting indirect excitons.

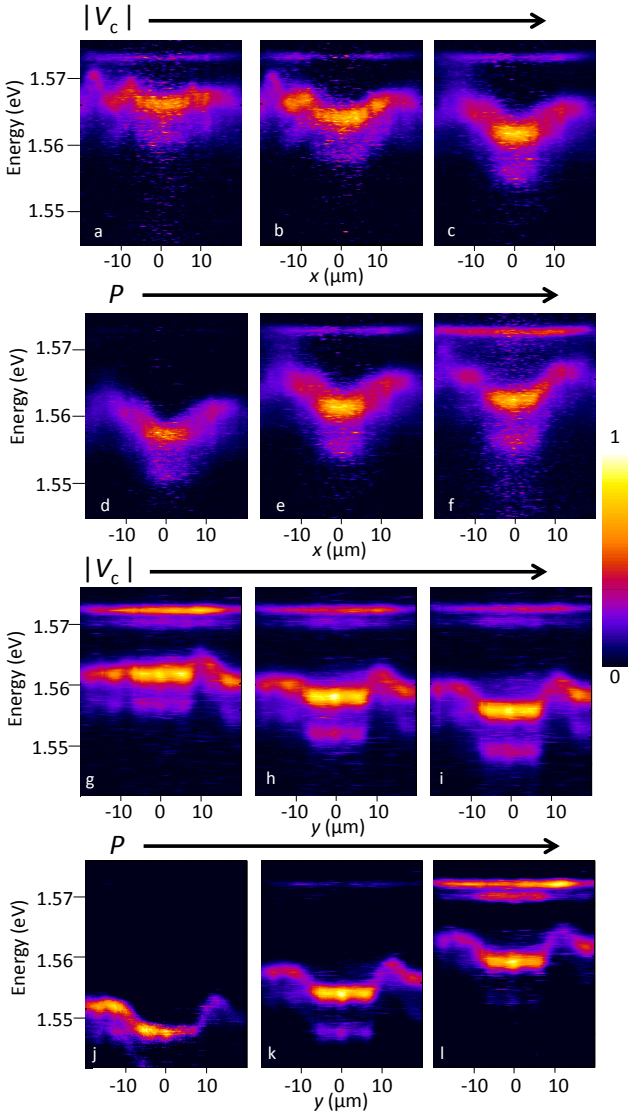

Figure 3.2: X-Energy Images of Trap: a-c, $x-$energy emission images vs center electrode voltage V_c. $V_c = -5$ (a,), -6.5 (b), and -8 (c) V. Outer electrode voltage $V_o = -6.5$ V, excitation power $P \sim 100\,\mu$W. g-i, Similar data for the orthogonal direction. d-f, $x-$energy emission images of indirect excitons vs P. $P \sim 20$ (d), 100 (e), and 500 (f) μW. $V_c = -8$ V, $V_o = -6.5$ V. j-l, Similar data for the orthogonal direction. For all data, a defocused laser excitation with the spot size $s = 40\,\mu$m is centered at the trap center. The emission at ~ 1.57 eV corresponds to spatially direct transitions. The emission of indirect excitons is observed at lower energies and is controlled by the trap potential and excitation power.

The repulsive interaction of indirect excitons originates from their built-in dipole moment [46]. Note however that even at the highest studied excitation powers the excitons do not screen the trap profile completely (Figs. 3.2d-f, 3.2j-l, and 3.3b,d).

The emission at ~ 1.57 eV corresponds to spatially direct transitions (Fig. 3.2). The spectra are measured in the defocused laser excitation spot. As discussed in the introduction [6, 17], typically, excitons are hot in the laser excitation spot and, as a result, direct exciton emission is present in the spectrum.

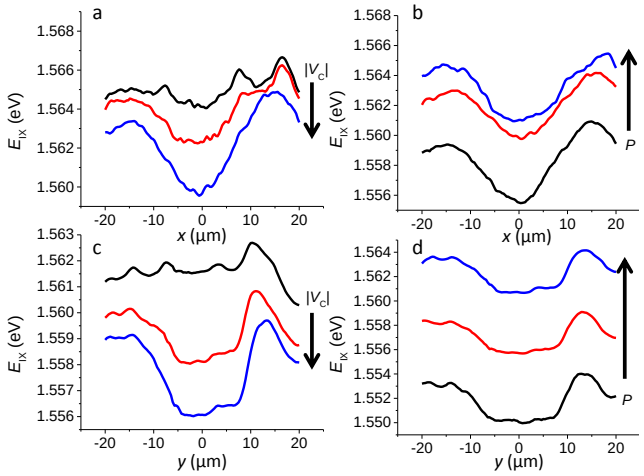

Figure 3.3: X-Energy Plots of Trap: a, Profiles of average energy of indirect excitons in the snowflake trap for different center electrode voltages V_c. $V_c = -5$, -6.5, and -8 V. Outer electrodes are at $V_o = -6.5$ V, excitation power $P \sim 100$ μW. b, Profiles of average energy of indirect excitons in the snowflake trap for different excitation powers P. $P \sim 20$, 100, and 500 μW. $V_c = -8$ V, $V_o = -6.5$ V. c-d, Similar data for the orthogonal direction. For all data, a defocused laser excitation with the spot size $s = 40$ μm is centered at the trap center.

The presented data demonstrate experimental proof of principle for snowflake traps. We note that the realized snowflake traps are not perfect: There is a disorder associated with the electrode imperfections originating from the electrode shape imperfections, surface charges, etc. The disorder is responsible for the deviation of the trap cross-section from the simulated profile and for the difference in the trap cross-sections in different directions. For instance, the trap cross-sections in the two orthogonal directions have different shapes (Fig. 3.2). However, the

disorder is not strong enough to compromise the major performance of the trap, namely, the ability to collect indirect excitons from all directions to the trap center (Fig. 3.1d). The emission appearing below the main indirect exciton line (Fig. 3.2) can be related to localized states in a disorder potential of the structure. Lower energy emission lines in the studied CQW structure typically correspond to localized states [18].

The quality of electrode shape and the performance of snowflake trap can be improved by increasing the lateral dimensions of the electrode pattern. For the same shape of the $x-y$ confining potential, the lateral dimensions can be increased by proportionally increasing the distances between the CQW and top and bottom electrodes [28]. Besides improving the trap quality, this can further increase the area of the confining potential: For instance, increasing D from 1 μm in the studied structure to 10 μm in future structures should increase the area of confining trap potential by two orders of magnitude. For a more efficient accumulation of indirect excitons to the center of such large traps, the lifetime of indirect excitons can be further enhanced by increasing the separation d between the QW layers. The development of snowflake traps forms the subject for future work.

3.2 Stirring Potential for Indirect Excitons

Controlled moving potentials are used for studying transport properties of excitons. An established method for creating moving potentials for excitons is based on surface acoustic waves (SAW). Transport of excitons, exciton-polaritons, and laterally separated electrons and holes via SAW has been realized [42, 44, 32, 8, 53, 33]. Large exciton transport distances in moving potentials can be achieved with indirect excitons composed of electrons and holes in spatially separated layers [Fig. 1(a)]: Indirect excitons have long lifetimes and can travel over large distances before recombination [15, 5, 31, 11, 23]. Effective transport of indirect excitons via SAW was demonstrated recently [44, 32, 53, 33].

Moving potentials for indirect excitons can also be created by laterally modulated AC voltage patterns. Indirect excitons have a built-in dipole moment ed (d is the separation between the electron and hole layers) so voltage-controlled electric field perpendicular to the QW plane F_z creates the desired potential landscape for indirect excitons $E(x,y) = -edF_z(x,y)$ [37]. Transport of indirect excitons was studied in static potentials formed by time-independent laterally modulated F_z, including ramps [15, 11, 34], lattices [40], traps [21, 54], and circuit devices [3]. Transport of indirect excitons in a moving electrostatic lattice potential – conveyer – was recently demonstrated [55]. The conveyer was created by applying AC voltages to the electrodes of an electrostatic lattice potential for excitons. This gave a traveling lattice moving indirect excitons laterally across the sample. The excitonic conveyer moves indirect excitons as charged coupled devices move electrons [52]. The moving wave of voltage couples to the dipole moment of indirect excitons in the former [55] and charge of electrons in the latter [52].

Voltage control allows the realization of a variety of moving potentials for indirect excitons. Stirring potentials are of particular interest. They can be used for studying rotating exciton matter. Optical and exciton-polariton systems with optically generated or spontaneously formed vorticity were intensively investigated, see [45, 38, 30, 27, 43] and references therein. Stirring was also explored in the studies of rotating atom matter, see [1, 50, 14] and references therein. In these diverse systems, stirring was explored to generate and study vortical states with angular momentum.

In this work, we present experimental proof of principle for a stirring potential for indirect excitons. Time-dependent voltage is applied to an electrode pattern deposited on top of the sample, resulting in a variable F_z in the CQW plane, and, in turn, a controllable potential landscape for indirect excitons $E(x,y,t)$.

A stirring (carousel) potential is created by a centrally symmetric set of semitransparent 11 nm thick Ti–Pt–Au electrodes on the sample surface. This is the same electrode pattern that was used to create the snowflake trap. The electrode width is 300 nm, carousel periodicity is 7

electrodes, and the angular wavelength of the carousel potential is $\theta_{car} = 45$ degrees [Fig. 3.4(c)].

AC voltages to the carousel electrodes are applied by coaxial cables with impedance-matching termination at the sample. The cable bandwidth complies with the frequency used

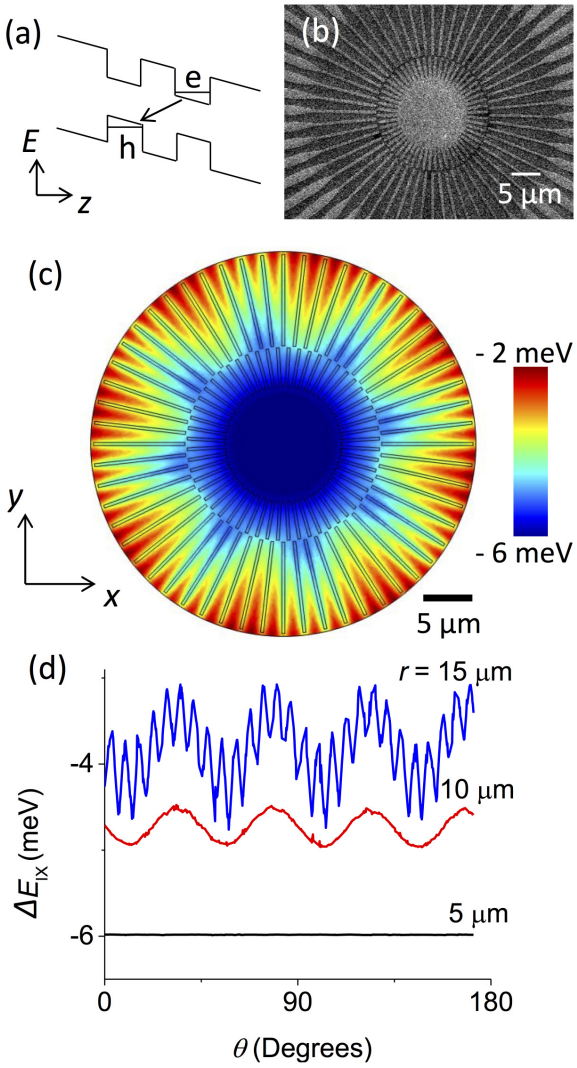

Figure 3.4: Diagrams and Simulations of Stirring Potential: (a) CQW diagram. e, electron; h, hole. An indirect exciton is shown by an arrow. (b) SEM image of the electrode pattern forming the stirring potential for indirect excitons. (c) Snapshot of calculated indirect exciton energy shift $E(x,y) = -edF_z$ in the stirring potential. (d) Angular cuts of calculated snapshot of indirect exciton energy shift at different radii. DC voltage on center and outer electrodes $V_c = V_o = .5$ V, AC voltage on outer electrodes $V_{AC} = 60$ mV. The stirring potential for indirect excitons rotates with the angular velocity $\omega_{car} = f\theta_{car}$ where f is the AC frequency and θ_{car} is the angular wavelength of the potential.

in the experiments. The regime where the indirect excitons form the ground state, i.e. have lower energy than spatially direct excitons in the CQW, is realized by DC biases V_c and V_o applied to the central electrode and outer set of electrodes, respectively. For $V_c = V_o$ used in the experiments, decreasing electrode density toward the carousel edges reduces F_z and, in turn, exciton energy shift, producing a confining potential for indirect excitons with the exciton energy reducing toward the carousel center [Figs. 3.4(c), (d)] [28]. A set of differentially phase-delayed AC voltage sine waves applied to the outer electrodes at frequency $f = 47.5$ MHz creates a stirring potential for indirect excitons – the excitonic carousel rotating with the angular velocity $\omega_{car} = f\theta_{car} \sim 2 \times 10^9$ degrees per second. The amplitude of the carousel potential for indirect excitons is controlled by the AC voltage V_{AC}. The radial dependence of the snapshot of the carousel potential is shown in Fig. 1(d). An effective stirring potential for indirect excitons is realized at the distance $r \sim 10$ μm from the center. At large $r \gtrsim 15$ μm, the sinusoidal envelope of the carousel potential with $\theta_{car} = 45$ degrees is modulated by ~ 6 degrees-period ripples, which originate from the finite spacing between the carousel electrodes d_s. The amplitude of these ripples is smaller for a smaller d_s, and the ripples essentially vanish at $r \sim 10$ μm where $d_s \lesssim 0.5$ μm for the structure [Figs. 3.4(c), (d)].

The sample mounts in a He cryostat at 1.5 K. The excitons are photoexcited by 700 nm Ti:sapphire laser focused to a spot ~ 6 μm in diameter at $r \sim 10$ μm. The exciton density is controlled by the laser excitation power P. Photoluminescence (PL) images of the exciton cloud are taken by a CCD with a bandpass filter 800 ± 5 nm covering the spectral range of the indirect excitons. The diffraction-limited spatial resolution is 1.4 μm.

Figure 3.5 presents experimental proof of principle for a stirring potential for indirect excitons. Figures 3.5(a) and (b) show $x-y$ PL images of indirect excitons for carousel off and on, respectively. The corresponding PL intensity profiles $I(\phi)$ presenting angular cuts of the emission images at $r = 15$ μm are shown on Fig. 3.5(c).

One could expect an emission pattern decaying monotonically with increasing angle from

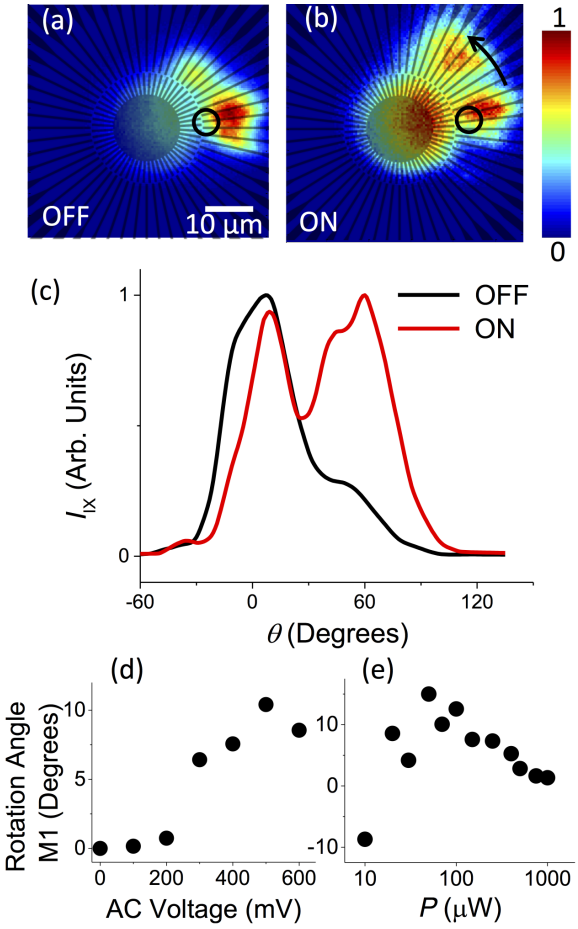

Figure 3.5: Images and Plots of Stirring Potential: (a)-(b) $x-y$ emission images of indirect excitons with AC voltage off and on. Excitation power $P = 50$ μW. Emission intensity in (b) is multiplied by a factor of 3.4 for clarity. Black circles show the excitation spot. The circle size corresponds to the excitation spot size.(c) Angular cuts of emission images in (a) and (b) at $r = 15$ μm. (d)-(e) The average rotation angle of indirect excitons via stirring potential M1 as a function of AC voltage V_{AC} (d) and excitation power P (e). $V_{AC} = 600$ mV in (a)-(c),(e). $P = 100$ μW in (d). For all data, DC center and outer voltage $V_c = V_o = 5$ V and AC frequency $f = 47.5$ MHz.

the excitation point. An enhancement of the emission at 60 degrees [Fig. 3.5(c)] is presumably related to a defect in the potential that can accumulate the exciton emission in its vicinity.

Switching on the rotating potential also leads to the enhancement of the emission at the center [Fig. 3.5(a-b)]. This can be understood as follows: Excitons are partly localized in the disorder in the structure; The rotating potential results in the exciton delocalization that, in turn, facilitates their motion toward the trap center.

The rotation of the exciton cloud by the carousel potential is presented by the extension of the exciton cloud along the angle of the stirring potential. We quantify it by the first moment of the PL intensity $M_1 = \int \phi I(\phi) d\phi / \int I(\phi) d\phi$, which characterizes the average rotation angle of indirect excitons via carousel. Figure 3.5(d) presents exciton cloud rotation via carousel as a function of the AC carousel voltage V_{AC} which controls the amplitude of the stirring potential. For a shallow carousel, the exciton cloud extension M_1 is not affected by the carousel rotation showing that the excitons do not follow the stirring potential. In contrast, at higher amplitude of the stirring potential, excitons are moved by the stirring potential. The exciton cloud starts to follow the conveyer and M_1 changes from constant to increasing with V_{AC} at $V_{AC} \sim 200$ mV [Fig. 3.5(d)]. These results can be understood as follows: When the carousel amplitude is smaller than the exciton interaction energy or amplitude of disorder (given by the intrinsic disorder in the structure and ripples in the conveyer potential), excitons are not localized in the minima of the rotating carousel potential, and therefore are not stirred by the carousel. When the carousel amplitude becomes larger than both the exciton interaction energy and disorder amplitude, excitons can localize in the minima of the rotating carousel potential. This results in efficient stirring of excitons via carousel. The transition between these two regimes is similar to the dynamical localization-delocalization transition for excitons in conveyers [55] and to the localization-delocalization transition for excitons in static lattices [40]: At low (high) amplitude of the stirring potential, excitons are dynamically delocalized (localized) in the stirring potential.

Figure 3.5(e) presents the dependence of exciton stirring via carousel on excitation density P. Efficient exciton stirring via carousel is achieved at intermediate densities and becomes less efficient at low and high densities. These results can be understood as follows: At low densities, the indirect excitons are localized in local minima of the disorder potential and hardly follow the rotating carousel. At the intermediate densities, excitons screen the disorder and can be efficiently stirred by the carousel. At the high densities, excitons screen the carousel potential that makes exciton stirring via carousel less efficient. In other words, excitons can efficiently follow

the stirring carousel potential when the exciton drift angular velocity in the carousel is higher than the carousel angular velocity $\omega_{\text{drift}} \gtrsim \omega_{\text{car}}$. For $\omega_{\text{drift}} \propto \mu U$ (μ is exciton mobility, U is the amplitude of stirring potential), an efficient exciton stirring is realized when both μ and U are high. Screening of disorder results in the enhancement of exciton mobility while screening of the stirring potential results in the reduction of the amplitude of the stirring potential.

3.3 Device Details

Sample description.

The structure was grown using molecular beam epitaxy. An n^+-GaAs layer with $n_{\text{Si}} = 10^{18}$ cm^{-3} serves as a homogeneous bottom electrode. A pair of 8 nm GaAs QWs, separated by a 4 nm $Al_{0.33}Ga_{0.67}As$ barrier, was positioned 0.1 μm above the n^+-GaAs layer within an undoped 1 μm thick $Al_{0.33}Ga_{0.67}As$ layer. Positioning the CQW closer to the homogeneous electrode suppresses the in-plane electric field [16], which otherwise can lead to exciton dissociation.

The top electrodes were fabricated as follows. Part of the sample was etched in order to connect to the homogeneous bottom electrode. The carousel layer was created by depositing a 7 nm Pt pattern with 2 nm Ti under layer for adhesion and 2 nm Au layer on top for increased electrical connectivity. This layer consists of a central snowflake-shaped static electrode and separate 300 nm wide lines that form outer electrodes (Fig 3.6a). A 200 nm insulating SiO_2 layer is deposited on top, leaving a 3 x 3 μm hole over each of the electrodes (Fig 3.6b). Connecting electrodes made of 200 nm thick ITO were deposited on top (Fig 3.6c), connecting the central electrode separately and every seventh outer electrode together. 700 nm wire-bondable Au pads with an ITO under layer were connected to both the ITO electrodes and the etched area of the sample, creating connections to each set of carousel electrode and the ground plane. Figure 3.7 shows a magnified version of the carousel electrodes with the insulating layer on top. Note the hole in the insulating layer for connection to the electrode layer.

Figure 3.8 shows the circuit diagram for the AC electronic system used to prevent reflections in the RF signal delivered to the electrodes in the carousel. Values for the resistors and capacitors are marked on the figure. AC voltages to the carousel electrodes on the sample are delievered via 7 broadband transmission lines with impedance-matching termination at the sample. We used coaxial cables UT-141B-SS silver-plated beryllium copper inner conductor, PTFE Teflon dielectric, and stainless-steel outer shell with diameter 3.6 mm, having a room-temperature attenuation of 3 dB/m at 10GHz. The cable bandwidth complies with the frequency used in the experiments, while the cable composition reduces heat conductance to the sample. The DC bias V_{bias} is supplied separately via regular wires. The transmission lines are capacitively terminated to block DC heating at the termination resistors.

3.4 Conclusion

In conclusion, we demonstrated experimental proof of principle for two-dimensional snowflake traps for indirect excitons which allow collecting a large number of excitons to the trap center. The operating principle of the snowflake trap is based on the lateral modulation of electrode density. We demonstrated collection of indirect excitons from all directions to the trap center and control of the trap shape by voltage. We also demonstrated experimental proof of principle for stirring potentials for indirect excitons, which allow for angular motion of excitons as they move around the center of a trap.

3.5 Acknowledgements

The text of chapter 3, in part, is a reprint of the material as it appears in Y.Y. Kuznetsova, P. Andreakou, M.W. Hasling, J.R. Leonard, E.V. Calman, L.V. Butov, M. Hanson, A.C. Gossard, Two-dimensional snowflake trap for indirect excitons, *Optics Letters*, 40, 589, 2015. The co-

authors in this publication directed, supervised, and co-worked on the research which forms the basis of this chapter. The text of chapter 3, in part, is a reprint of the material as it appears in M.W. Hasling, Y.Y. Kuznetsova, P. Andreakou, J.R. Leonard, E.V. Calman, C.J. Dorow, L.V. Butov, M. Hanson, A.C. Gossard, Stirring potential for indirect excitons, *Journal of Applied Physics*, 117, 023108, 2015, where the dissertation author was the first author. The co-authors in this publication directed, supervised, and co-worked on the research which forms the basis of this chapter.

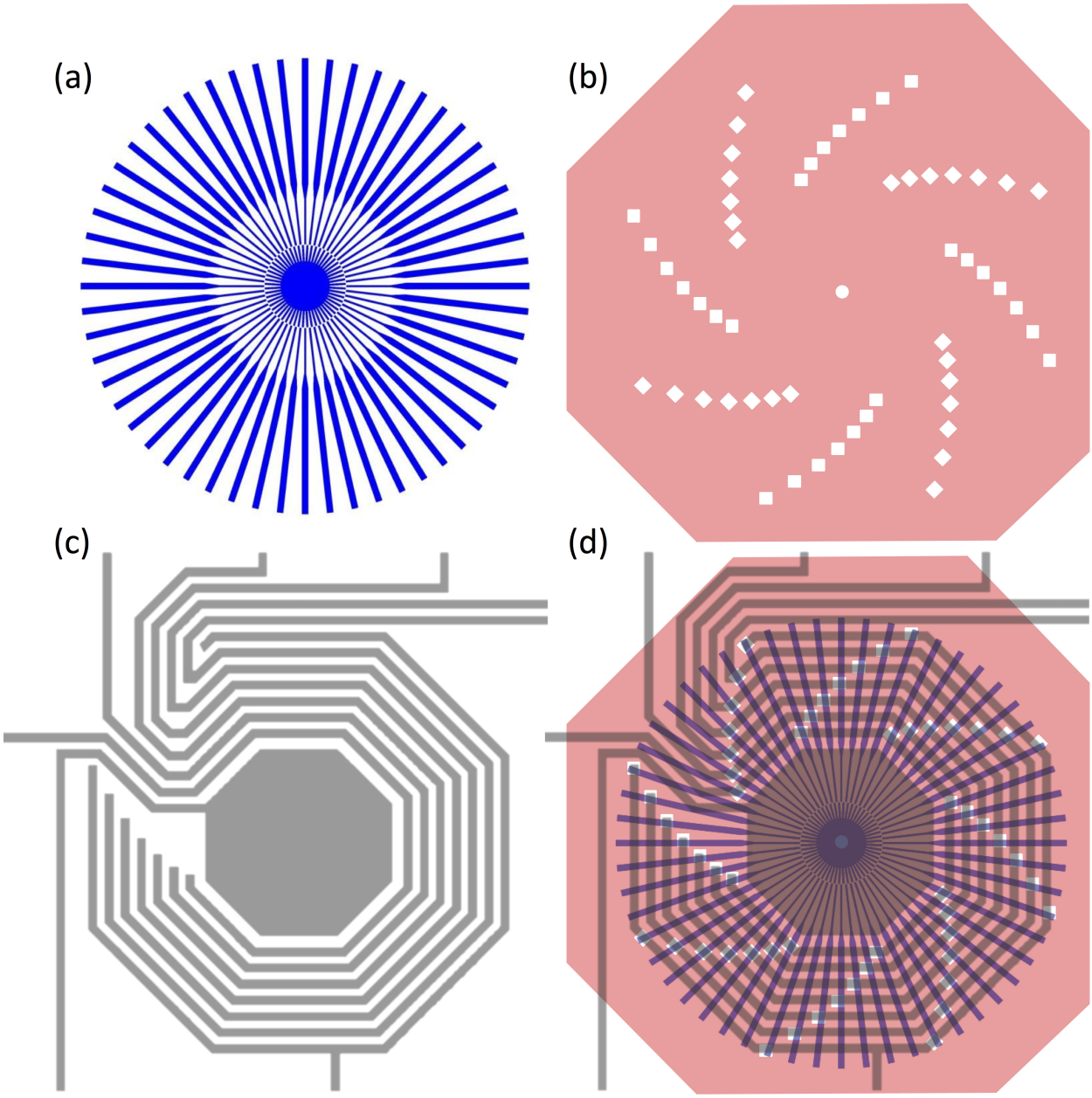

Figure 3.6: Layers that form the carousel: (a) Platinum electrodes (b) SiO_2 insulating layer (c) ITO connecting electrodes (d) All 3 layers overlaid. White circles indicate where the gaps in the insulating layer are.

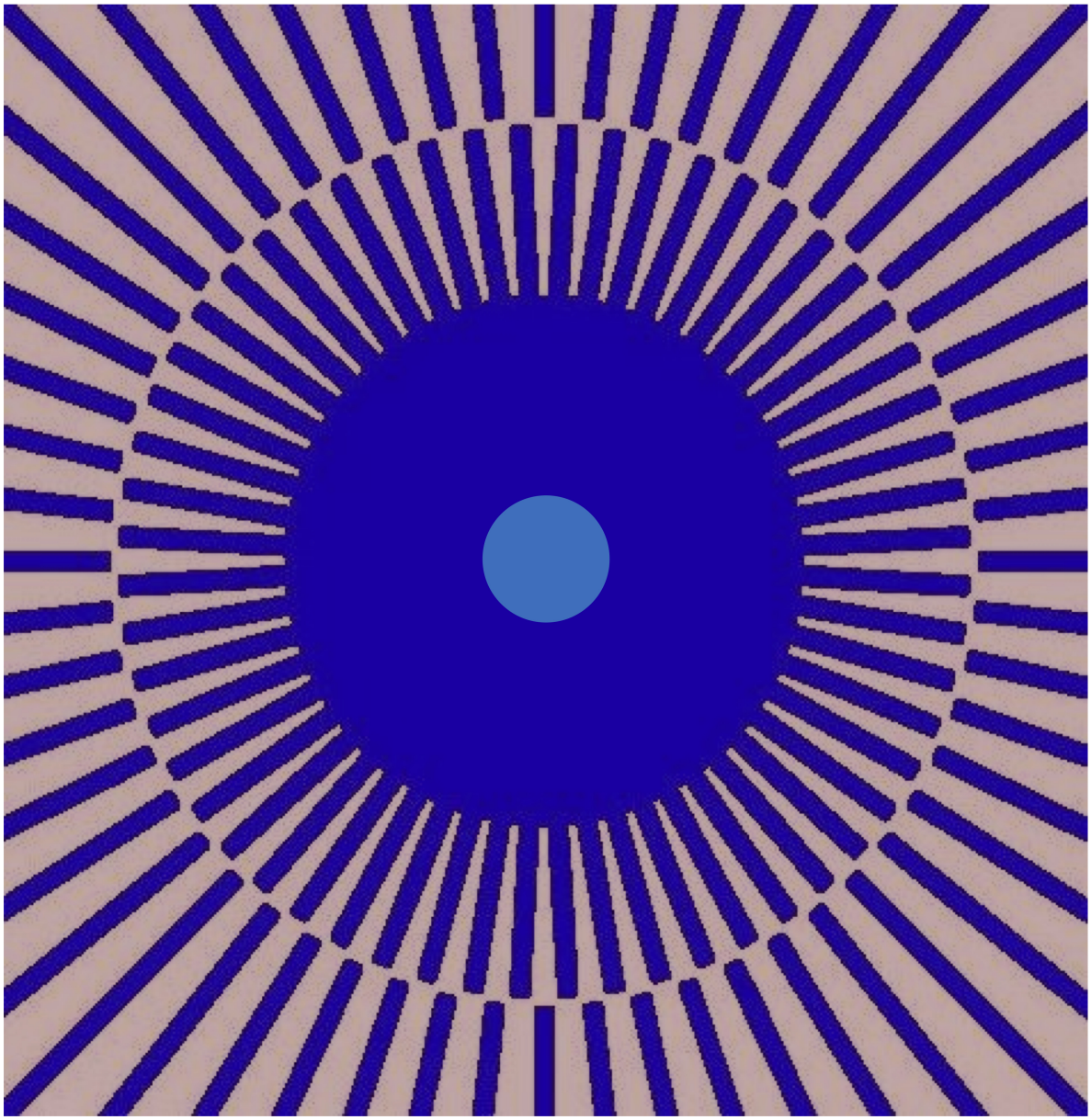

Figure 3.7: Magnified view of carousel electrodes and insulating layer.

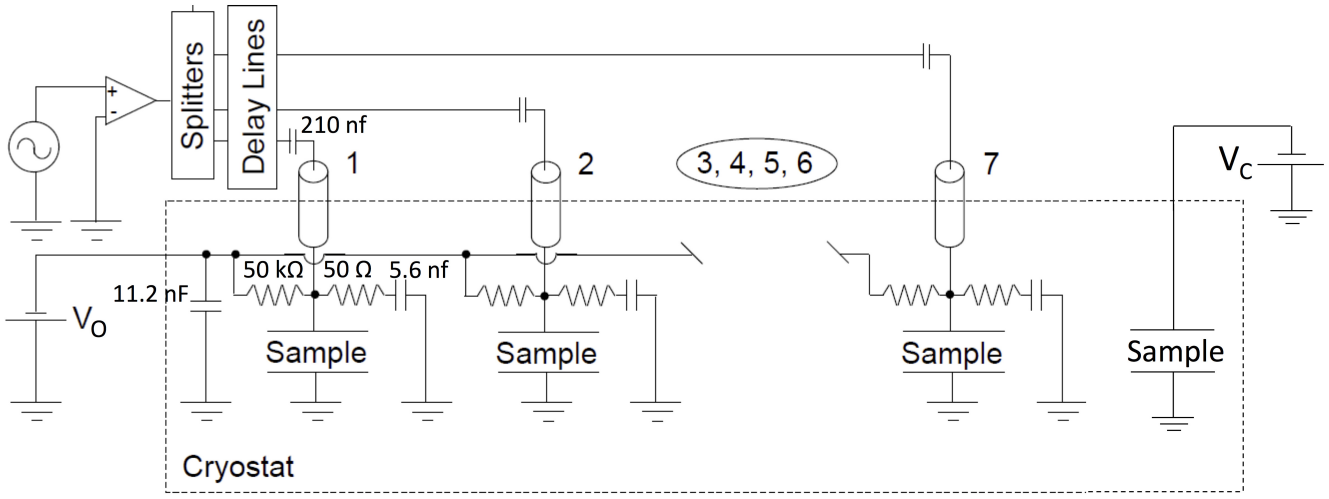

Figure 3.8: Circuit Schematic: Circuit schematic for the entire carousel system with seven electrode lines.

Chapter 4

Development of Imaging Spectroscopy at Ultra-Low Temperatures

Whan working in any experimental lab, a large part of the work is building the equipment necessary to perform the desired experiments. This equipment often needs to be made specially for the setups that already exist in a lab, so the designs must be very specialized. I spent a large part of my time building and installing equipment for the lab, and this section details those endeavors.

4.1 Piezoelectric Stage

With any optical setup, the component closest to the object being imaged is known as the objective. Typical objective focal lengths range from a few centimeters to a few millimeters. Because of this, in the dilution refrigerator setup, the objective must sit inside the fridge with the sample. This presents an experimental difficulty, because this removes the ability to focus the objective $in-situ$. Also, focusing the objective at room temperature is not sufficient, because the thermal contraction of the materials in the fridge is enough to shift the focus on the order of a

millimeter. In the past, experiments were conducted by approximating this contraction and then compensating for the slightly out of focus objective with a collection telescope outside of the fridge. This is, of course, suboptimal, and a better solution was required. In order to overcome this obstacle, adding a piezoelectric stage to the setup became the logical next step, as that is one of the few motors that can function at low temperatures. The stage functions on a slip-grip principle, where the piezo material slowly expands and then quickly contracts, driven by a saw wave from a signal generator, as shown in Figure 4.1.

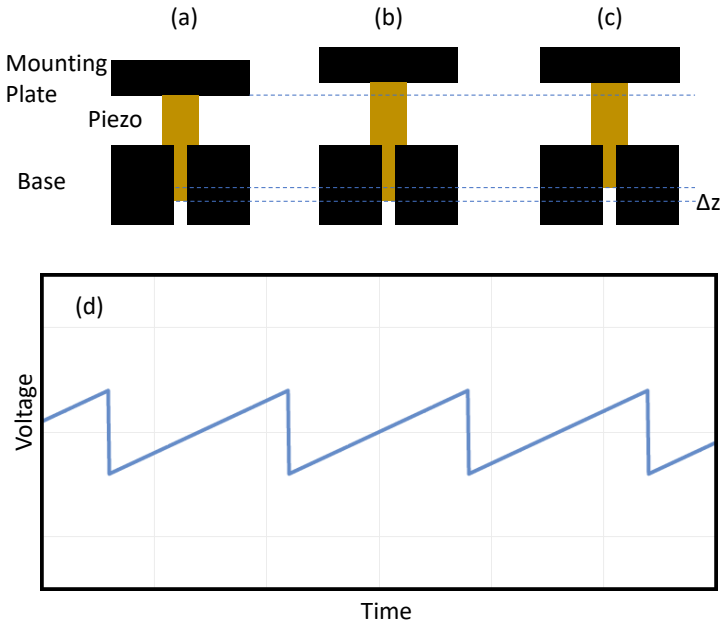

Figure 4.1: Demonstration of piezoelectric stage motion: (a) Initial state of the stage (b) With applied voltage slowly increasing, the piezoelectric material slowly expands (c) The voltage quickly drops, and the piezoelectric material rapidly contracts, slipping on the base clamp (d) Spatial representation of the saw wave applied to the piezoelectric material.

The critical element in all of this is that the friction between the base and the the element sliding through it is such that it will slip during the rapid contraction, but not during the slow expansion. This can be accomplished by attaching the peizoelectric material to a graphite bar, and having the graphite be the portion that slides through the base. The base is most

commonly made from titanium, but titanium creates a potential problem, because titanium becomes superconducting at temperatures below 0.4K. This would interfere with any experiments conducted in the area involving electronic measurements, so would not be conducive to our needs. Therefore, it was necessary to use another material commonly used in piezoelectric stages, beryllium copper. It is important to note that beryllium copper is toxic when inhaled, so any machining of the material must be done very carefully to ensure that no dust generated can be inhaled. For this purpose, all machining of parts was done at the UCSD Scripps Institute of Oceanography Marine Science Development Center, under the supervision of Ken Duff. The structure of the designed piezoelectric stage included 6 different components: The piezoelectric element, the graphite bar, two clamping pieces, the spacer, and the mounting block. The drawings for each piece are shown in Figures 4.2-6, and the completed stage construction is shown in Figure 4.7.

The key element to the slip-grip motion is the frictional force between the beryllium copper clamp element and the graphite bar. This force can be adjusted by two main factors: The tightness of the screws between the clamp pieces and the roughness of the surface of the graphite and beryillium copper. However, neither of these factors can be changed once the setup has been placed inside a cryostat. Many iterations of this frictional force were tested, but as the temperature decreased, the amplitude of the saw wave applied to the stage needed to move the stage increased, as shown in Figure 4.8. The signal generator in the setup was limited to an amplitude of 150V, so exceeding that was not possible. The desired temperature of operation was at 1K in the dilution refrigerator setup, so this device would not be able to be moved into that setup until motion could be produced at 1K.

After many iterations of adjusting the friction between the graphite bar and the clamp element, it became clear that the more efficient course of action would be to purchase a similar piezoelectric stage from the company Attocube. A sample mount was constructed for this stage, and this new device was then added to the dilution refrigerator setup, as shown in Figure 4.9. The

stage design shown here can still be used for many measurements done in other setups at room temperature, particularly those in which objective focus is sensitive.

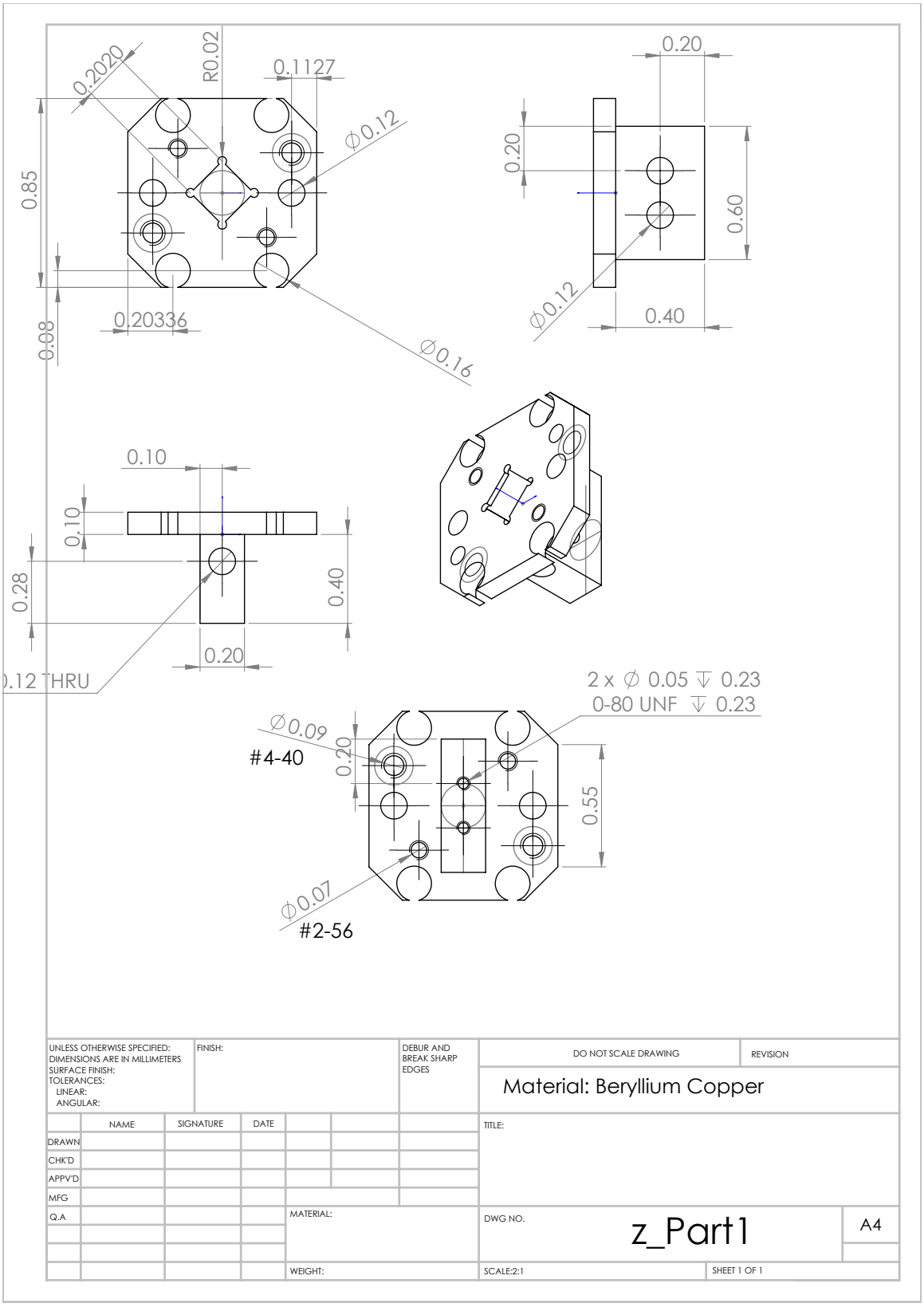

Figure 4.2: Stage Mounting Block: The mounting block for attaching the sample, as well as copper braids for better thermal conductivity and temperature sensors.

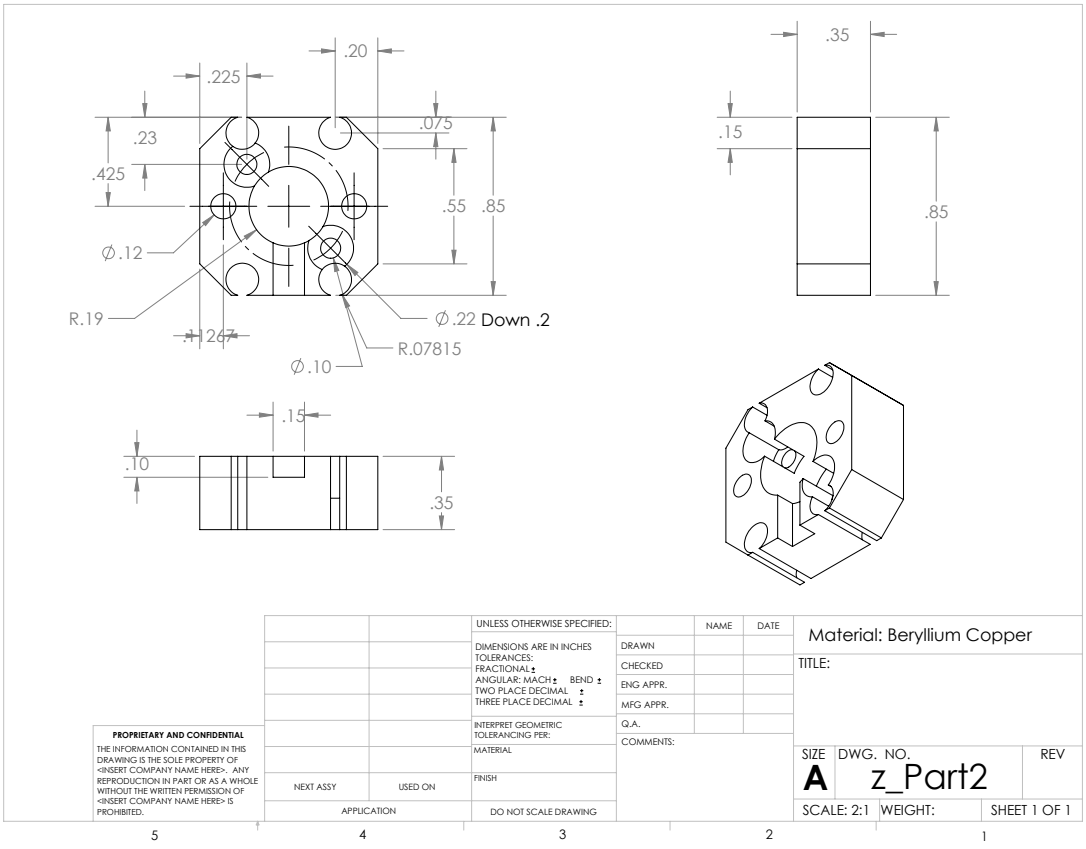

Figure 4.3: Stage Spacer: The spacer between the clamp elements and the mounting block. This part also gives the moving piece additional mass, which allows for more effective slipping during that part of the motion.

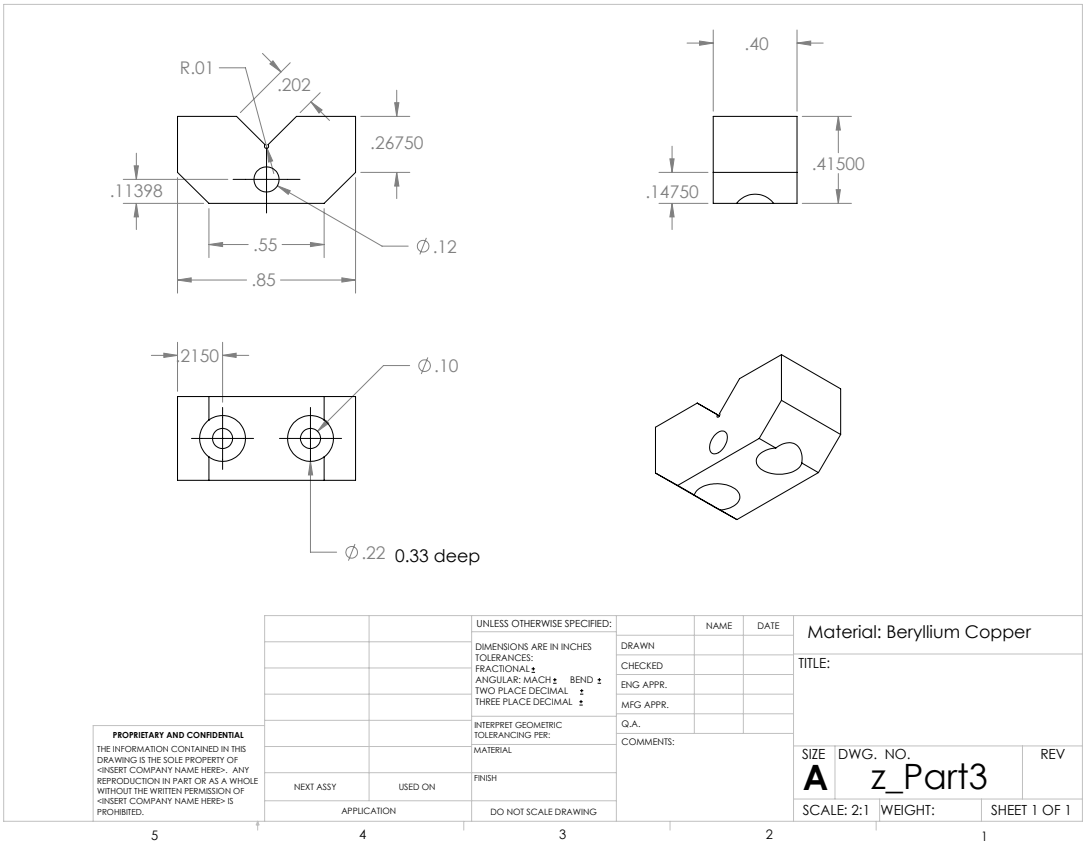

Figure 4.4: Stage Clamp 1: One side of the clamp element that produces the pressure necessary to create the friction needed for the slip-grip motion. This side has through holes where screws pass through, threading into the other clamp piece.

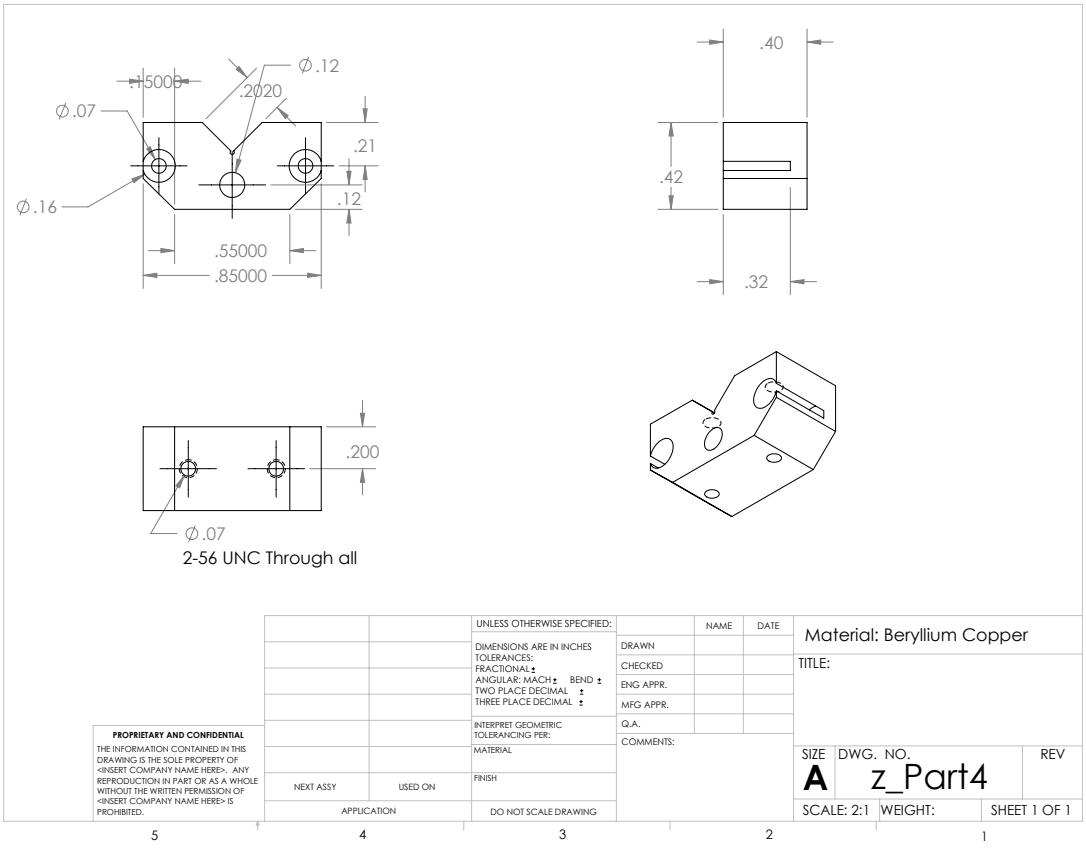

Figure 4.5: Stage Clamp 2: The second part of the clamp element. This side is threaded with 2-56 screw holes, allowing for screws that can be tightened as needed to produce the desired frictional force.

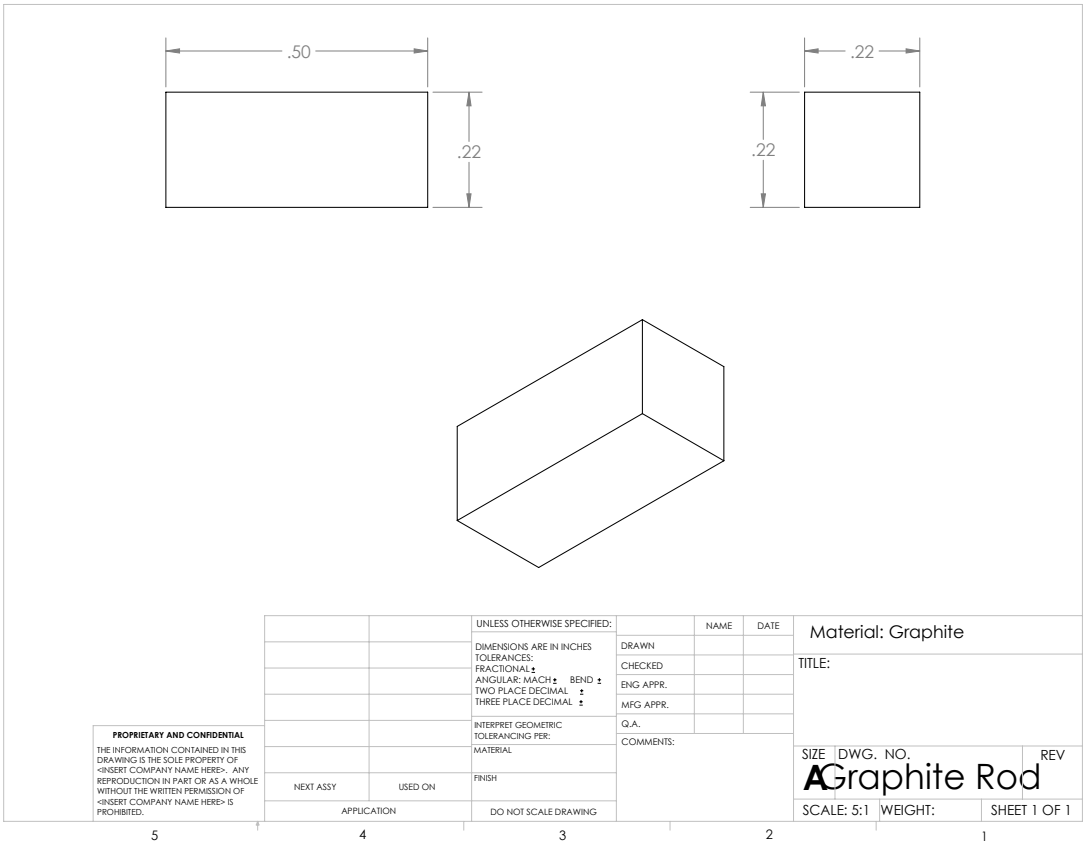

Figure 4.6: Graphite Bar: The graphite bar that slides between the clamp pieces. The friction between this piece and the beryllium copper clamp is the crux of the slip-grip motion.

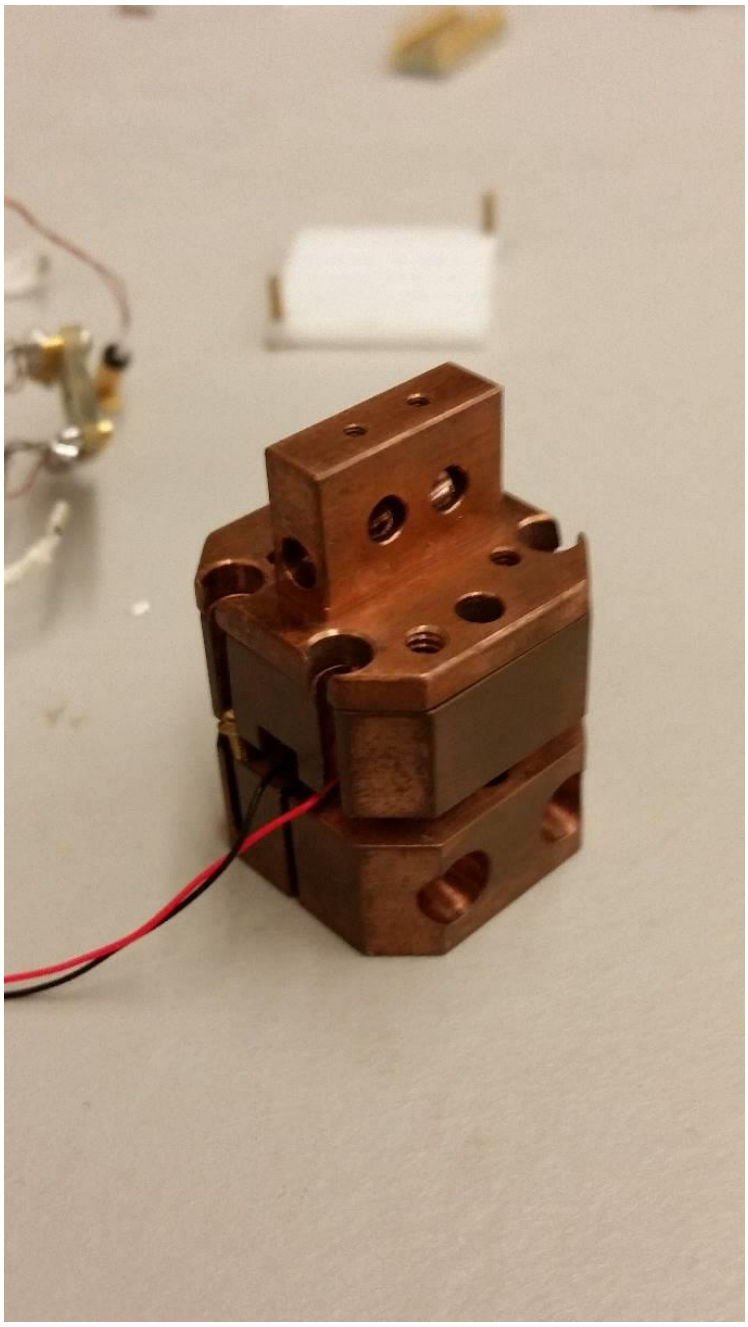

Figure 4.7: Constructed Stage: The final constructed piezoelectric stage.

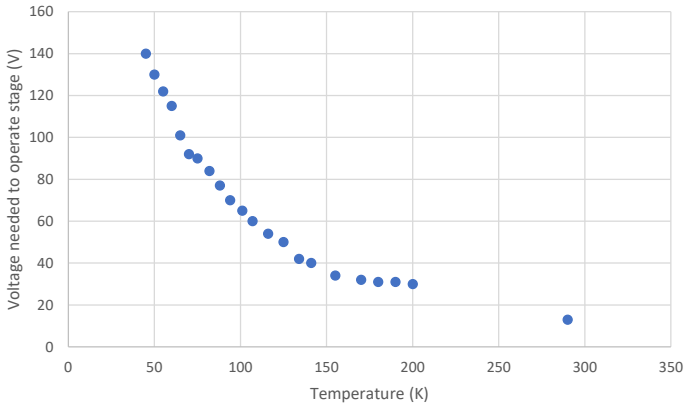

Figure 4.8: Stage Amplitude Plot: Typical curve of the saw wave amplitude needed to move the stage.

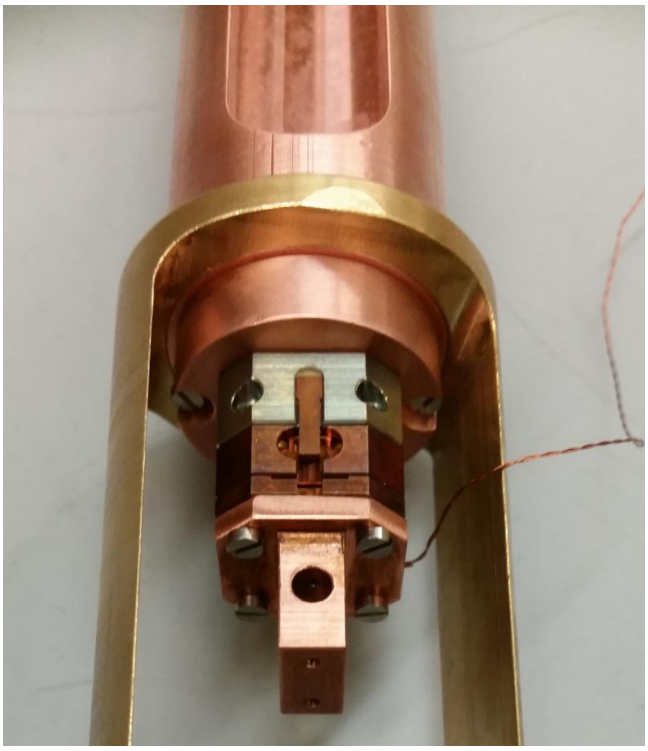

Figure 4.9: Completed Design: Attocube stage with mounting plate and sample mount. This setup is now in the dilution fridge experimental setup.

Chapter 5

Wide Single Quantum Well

The previous work discussed in this thesis was performed with GaAs samples that contained two coupled quantum wells. However, indirect excitons can still be formed in a wide single quantum well, as shown in Figure 6.1. In this work, we present a new platform for the study of indirect excitons, in the form of a low-disorder GaAs single QW structure. Two samples were tested in this study, with different thicknesses between the QW and the doped region, labeled sample 1 and sample 2, as shown in Figure 5.1(d)-(e).

Impurities in a QW structure manifest in small energy minima and maxima, creating an uneven energy landscape, and causing localization of indirect excitons. This is referred to as disorder in a sample. Disorder in QW structures limits mobility of indirect excitons, which is reflected in the diffusion coefficient of a growing exciton cloud. The sample presented in this study was grown using molecular beam epitaxy to produce a sample with high purity and low disorder.

Studies on the sample were conducted using two different experimental setups: Initial measurements were made using continuous Helium Neon (633nm) excitation and a nitrogen cooled CCD, and time resolved measurements were made using a pulsed semiconductor laser (640nm) and a gated intensifier before the CCD. The gated intensifier allows for the exciton

signal to be collected during a 10ns window somewhere in the duration of the laser pulse period. This window can be shifted through the entire duration of the laser pulse period, so images of the exciton cloud expanding at the beginning of the pulse and fading after the pulse can be taken. The pulse is shown in Figure 5.1(a), with the laser on for 2 μs and off for 4 μs.

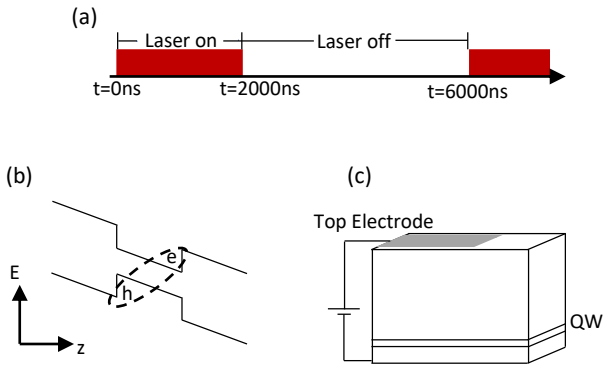

Figure 5.1: Diagrams of Setup: (a) Representation of laser pulse. The pulse has a period of 6 μs, with the laser on for 2 μs and off for 4 μs. (b) Diagram of an indirect exciton in a single quantum well. (c) Diagram of sample structure. Electrodes on the top and bottom of sample provide the electric field needed.

Figure 5.2 shows control of IX energy by voltage. As is shown in figure 5.2(a), the exciton energy shift is 14.5 meV/V. This holds true for both samples tested, and for excitation powers ranging from 0.1 μW to 20 μW.

Figure 5.3(a)-(e) shows x-energy images of the exciton cloud expanding over time. These images were taken on sample 2, with an excitation power of 20 μW. The exciton cloud expands over the course of roughly 200 ns, which is the lifetime of the indirect excitons. Figure 5.3(f) shows a plot of the decaying intensity of the IX cloud after the laser has been turned off, demonstrating that lifetime.

Plotting the area of the IX cloud as it expands is an effective way to calculate the diffusion

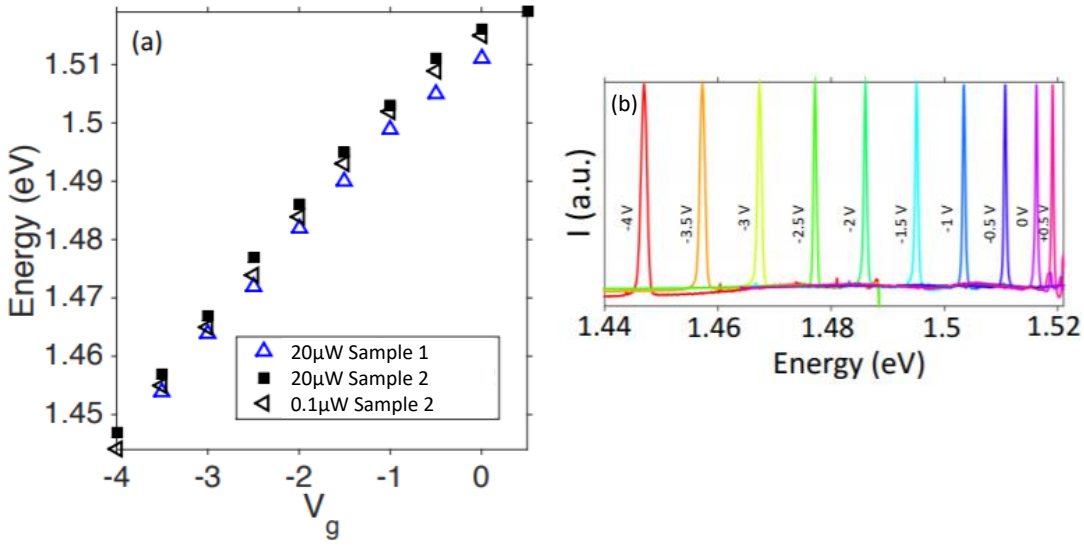

Figure 5.2: Demonstration of Voltage Control: (a) Plot of IX energy peak as a function of gate voltage. Data from both samples with 20 μW excitation power is shown, as well as data from sample 2 at 0.1 μW excitation power. (b) IX spectra for varying voltage on sample 2, with 20 μW excitation power.

coefficient of a sample. However, the expansion of the IX cloud can be modeled several ways. Here, we estimate the diffusion coefficient for the sample by applying a linear fit of $R^2 - R_0^2 = Dt$ to the initial expansion period, where R_0 is the excitation spot radius. Using this estimation, we can calculate an approximate diffusion coefficient of 270 cm^2/s. This is significant, as previous diffusion coefficients studied in CQW structures were approximately 90 cm^2/s, and this is a considerable improvement on that aspect.

This sample also demonstrates a narrow energy line width for IX. As shown in Figure 5.5(a), the IX energy line width in these samples is lower than 0.6meV.

A large diffusion coefficient (Figure 5.4), narrow line width (Figure 5.5), and excellent tunability of energy (Figure 5.2) are quite desirable qualities in a sample used for creating excitonic devices and for studying basic properties of indirect excitons. Both properties indicate low disorder in a sample, which means that indirect excitons can move through the sample more

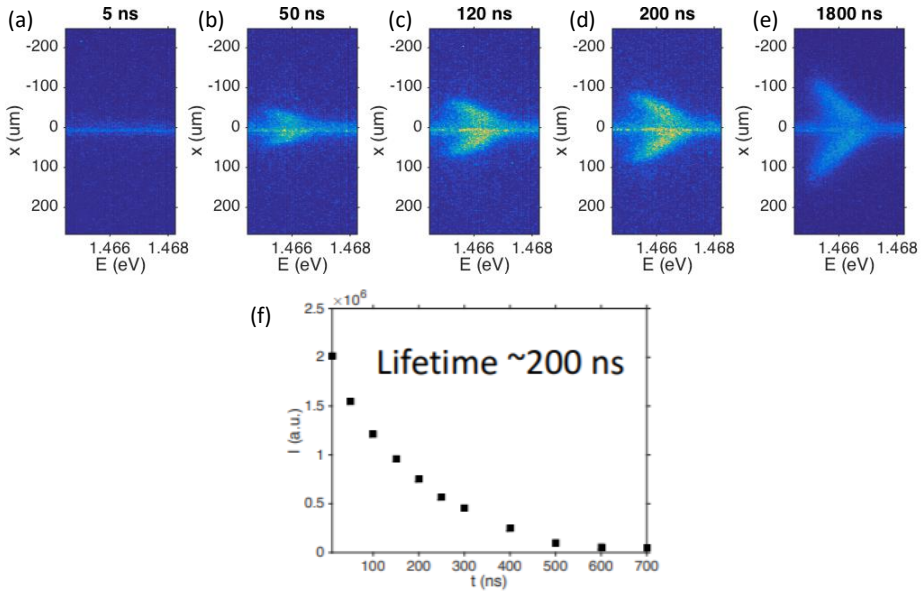

Figure 5.3: Expanding and Decaying IX: (a)-(e) x-Energy images of the expanding IX cloud on sample 2, with an excitation power of 20uW and a gate voltage of -3V. (f) Integrated intensity of IX cloud after pulse has been turned off, plotted over time.

effectively. This new structure can serve as a new platform for the study of indirect excitons, and allow for the development of new excitonic devices.

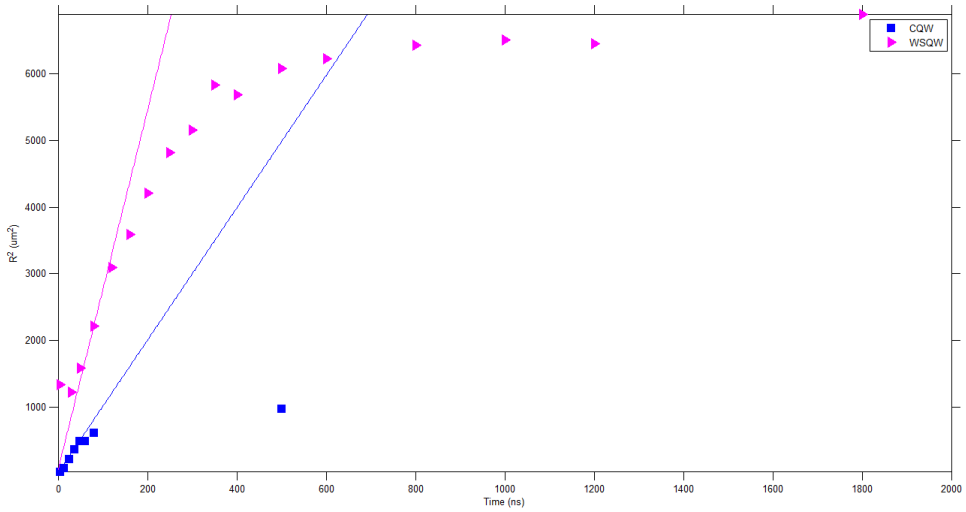

Figure 5.4: Diffusion Plots: Plot of the area of the IX cloud over time for the WSQW sample, as well as similar data for previous CQW samples. The $R^2 - R_0^2 = Dt$ fits of the early expansion period for both samples are shown. These lines correspond with an approximate diffusion coefficient of D$\sim$270 cm^2/s on the WSQW sample, and D$\sim$90 cm^2/s on the CQW sample.

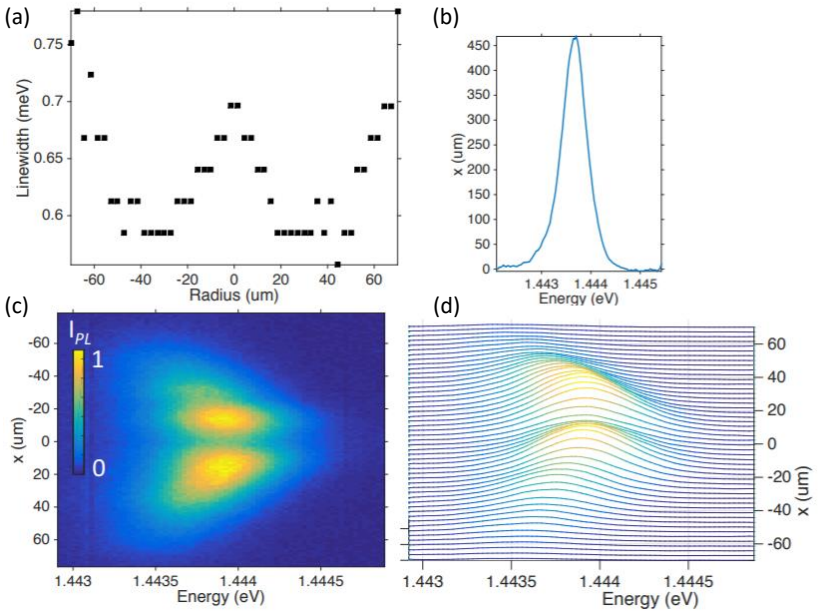

Figure 5.5: Plots of IX Line Width: (a) Plot of IX energy line width over the full radius of the IX cloud. (b) Plot of the narrow IX line width at R=30μm. (c) x-energy image of exciton cloud immediately after laser has been turned off. (d) Spectra of IX as a function of distance from the excitation spot.

Bibliography

[1] J. R. Abo-Shaeer, C. Raman, J. M. Vogels, and W. Ketterle. Observation of vortex lattices in bose-einstein condensates. *Science*, 292:476, 2001.

[2] G. M. Akselrod, P. B. Deotare, N. J. Thompson, Jiye Lee, W. A. Tisdale, M. A. Baldo, V. M. Menon, and V. Bulović. Visualization of exciton transport in ordered and disordered molecular solids. *Nature Commun.*, 5:3646, 2014.

[3] P. Andreakou, S. V. Poltavtsev, J. R. Leonard, E. V. Calman, M. Remeika, Y. Y. Kuznetsova, L. V. Butov, J. Wilkes, M. Hanson, and A. C. Gossard. Optically controlled excitonic transistor. *Appl. Phys. Lett.*, 104:091101, 2014.

[4] L.C. Andreani, F. Tassone, and F. Bassani. Radiative lifetime of free excitons in quantum wells. *Solid State Comm.*, 77(9):641645, 1991.

[5] L. V. Butov and A. I. Filin. Anomalous transport and luminescence of indirect excitons in alas/gaas coupled quantum wells as evidence for exciton condensation. *Phys. Rev. B*, 58:1980, 1998.

[6] L. V. Butov, A. L. Ivanov, A. Imamoglu, P. B. Littlewood, A. A. Shashkin, V. T. Dolgopolov, K. L. Campman, and A. C. Gossard. Stimulated scattering of indirect excitons in coupled quantum wells: Signature of a degenerate bose-gas of excitons. *Phys Rev. Lett.*, 86:5608, 2001.

[7] L.V. Butov, A.C. Gossard, and D.S. Chemla. Macroscopically ordered state in exciton system. *Nature*, 417:751, 2002.

[8] E. A. Cerda-Mendez, D. N. Krizhanovskii, M. Wouters, R. Bradley, K. Biermann, K. Guda, R. Hey, P. V. Santos, D. Sarkar, and M. S. Skolnick. Polariton condensation in dynamic acoustic lattices. *Phys. Rev. Lett.*, 105:116402, 2010.

[9] G. Chen, R. Rapaport, L. N. Pffeifer, K. West, P. M. Platzman, S. Simon, Z. Vörös, and D. Snoke. Artificial trapping of a stable high-density dipolar exciton fluid. *Phys Rev. B*, 74:045309, 2006.

[10] C.J. Dorow, Y.Y. Kuznetsova, J.R. Leonard, M.K. Chu, L.V. Butov, J. Wilkes, M. Hanson, and A.C. Gossard. Indirect excitons in a potential energy landscape created by a perforated electrode. *Appl. Phys. Lett.*, 108:073502, 2016.

[11] A. Gartner, A. W. Holleitner, J. P. Kotthaus, and D. Schuh. Drift mobilitiy of long-living excitons in coupled gaas quantum wells. *Appl. Phys. Lett.*, 89:052108, 2006.

[12] A.V. Gorbunov and V.B. Timofeev. Interwell excitons in a lateral potential well in an inhomogeneous electric field. *JETP Letters*, 80:185189, 2004.

[13] G. Grosso, J. Graves, A. T. Hammack, A. A. High, L. V. Butov, M. Hanson, and A. C. Gossard. Excitonic switches operating at around 100 k. *Nature Photonics*, 3:577, 2009.

[14] Z. Hadzibabic, P. Krüger, M. Cheneau, B. Battelier, and J. Dalibard. Berezinskii-kosterlitz-thouless crossover in a trapped atomic gas. *Nature*, 441:1118, 2006.

[15] M. Hagn, A. Zrenner, G. Bohm, and G. Weimann. Electric-field-induced exciton transport in coupled quantum well structures. *Appl. Phys. Lett.*, 67:232, 1995.

[16] A. T. Hammack, N. A. Gippius, Sen Yang, G. O. Andreev, L. V. Butov, M. Hanson, and A. C. Gossard. Excitons in electrostatic traps. *J. Appl. Phys.*, 99:066104, 2006.

[17] A. T. Hammack, M. Griswold, L. V. Butov, L. E. Smallwood, A. L. Ivanov, and A. C. Gossard. Trapping of cold excitons in quantumwell structures with laser light. *Phys Rev. Lett.*, 96:227402, 2006.

[18] A. A. High, A. T. Hammack, L. V. Butov, L. Mouchliadis, A. L. Ivanov, M. Hanson, and A. C. Gossard. Indirect excitons in elevated traps. *Nano Lett.*, 9:2094, 2009.

[19] A. A. High, J. R. Leonard, M. Remeika, L. V. Butov, M. Hanson, and A. C. Gossard. Condensation of excitons in a trap. *Nano Lett.*, 12:2605, 2012.

[20] A. A. High, E. E. Novitskaya, L. V. Butov, M. Hanson, and A. C. Gossard. Control of exciton fluxes in an excitonic integrated circuit. *Science*, 321:229, 2008.

[21] A. A. High, A. K. Thomas, G. Grosso, M. Remeika, A. T. Hammack, A. D. Meyertholen, M. M. Fogler, L. V. Butov, M. Hanson, and A. C. Gossard. Trapping indirect excitons in a gaas quantum-well structure with a diamond-shaped electrostatic trap. *Phys. Rev. Lett.*, 103:087403, 2009.

[22] T. Huber, A. Zrenner, W. Wegscheider, and M. Bichler. Electrostatic exciton traps. *Phys Status Solidi A*, 166, 1998.

[23] A. L. Ivanov, L. E. Smallwood, A. T. Hammack, Sen Yang, L. V. Butov, and A. C. Gossard. Origin of the inner ring in photoluminescence patterns of quantum well excitons. *Europhys. Lett.*, 73:920, 2006.

[24] A.L. Ivanov. Quantum diffusion of dipole-oriented indirect excitons in coupled quantum wells. *Europhys. Lett.*, 59(4):586–591, 2002.

[25] K. Kowalik-Seidl, X. P. Vögele, B. N. Rimpfl, G. J. Schinner, D. Schuh, W. Wegscheider, A. W. Holleitner, and J. P. Kotthaus. Tunable photoemission from an excitonic antitrap. *Nano Lett.*, 12:326, 2012.

[26] J. Krauß, J. P. Kotthaus, A. Wixforth, M. Hanson, D. C. Driscoll, A. C. Gossard, D. Schuh, and M. Bichler. Capture and release of photonic images in a quantum well. *Appl Phys. Lett.*, 85:5830, 2004.

[27] D. N. Krizhanovskii, D. M. Whittaker, R. A. Bradley, K. Guda, D. Sarkar, D. Sanvitto, L. Vina, E. Cerda, P. Santos, K. Biermann, R. Hey, and M. S. Skolnick. Effect of interactions on vortices in a nonequilibrium polariton condensate. *Phys. Rev. Lett.*, 104:126402, 2010.

[28] Y. Y. Kuznetsova, A. A. High, and L. V. Butov. Control of excitons by laterally modulated electrode density. *Appl. Phys. Lett.*, 97:201106, 2010.

[29] Y. Y. Kuznetsova, J. R. Leonard, L. V. Butov, J. Wilkes, E. A. Muljarov, K. L. Campman, and A. C. Gossard. Excitation energy dependence of the exciton inner ring. *Phys. Rev. B*, 85:165452, 2012.

[30] K. G. Lagoudakis, T. Ostatnicky, A. V. Kavokin, Y. G. Rubo, R. Andre, and B. Deveaud-Pledran. Observation of half-quantum vortices in an exciton-polariton condensate. *Science*, 974, 2009.

[31] A. V. Larionov, V. B. Timofeev, J. Hvam, and K. Soerensen. Interwell excitons in gaas/algaas double quantum wells and their collective properties. *JETP*, 1093, 2000.

[32] S. Lazic, P. V. Santos, and R. Hey. Exciton transport by moving strain dots in gaas quantum wells. *Physica (Amsterdam)*, 2640, 2010.

[33] S. Lazic, A. Violante, K. Cohen, R. Hey, R. Rapaport, and P. V. Santos. Scalable interconnections for remote indirect exciton systems based on acoustic transport. *Phys. Rev. B*, 89:085313, 2014.

[34] J. R. Leonard, M. Remeika, M. K. Chu, Y. Y. Kuznetsova, A. A. High, L. V. Butov, J. Wilkes, M. Hanson, and A. C. Gossard. Transport of indirect excitons in a potential energy gradient. *Appl. Phys. Lett.*, 100:231106, 2012.

[35] S.V. Lobanov, N.A. Gippius, and L.V. Butov. Theory of condensation of indirect excitons in a trap. *Phys. Rev. B*, 94:245401, 2016.

[36] Y. Mazuz-Harpaz, K. Cohen, B. Laikhtman, R. Rapaport, K. West, and L.N. Pfeiffer. Radiative lifetimes of dipolar excitons in double quantum wells. *Phys. Rev. B*, 95:155302, 2017.

[37] D. A. B. Miller, D. S. Chemla, T. C. Damen, A. C. Gossard, W. Wiegmann, T. H. Wood, and C. A. Burrus. Electric field dependence of optical absorption near the band gap of quantum-well structures. *Phys. Rev. B*, 32:1043, 1985.

[38] M. Padgett, J. Courtial, and L. Allen. Light's orbital angular momentum. *Physics Today*, 35, May 2004.

[39] M. Remeika, M. M. Fogler, L. V. Butov, M. Hanson, and A. C. Gossard. Two-dimensional electrostatic lattices for indirect excitons. *Appl Phys. Lett.*, 100:061103, 2012.

[40] M. Remeika, J. C. Graves, A. T. Hammack, A. D. Meyertholen, M. M. Fogler, L. V. Butov, M. Hanson, and A. C. Gossard. Localization-delocalization transition of indirect excitons in lateral electrostatic lattices. *Phys. Rev. Lett.*, 102:186803, 2009.

[41] M. Remeika, J.R. Leonard, C.J. Dorow, M.M. Fogler, L.V. Butov, M. Hanson, and A.C. Gossard. Measurement of exciton correlations using electrostatic lattices. *Phys. Rev. B*, 92:115311, 2015.

[42] C. Rocke, S. Zimmermann, A. Wixforth, J. P. Kotthaus, G. Bohm, and G. Weimann. Acoustically driven storage of light in a quantum well. *Phys Rev. Lett.*, 78(4099), 1997.

[43] G. Roumpos, M. D. Fraser, A. Löffler, S. Höfling, A. Forchel, and Y. Yamamoto. Single vortex-antivortex pair in an exciton-polariton condensate. *Nature Physics*, 7:129, 2011.

[44] J. Rudolph, R. Hey, and P. V. Santos. Long-range exciton transport by dynamic strain fields in a gaas quantum well. *Phys. Rev. Lett.*, 99(047602), 2007.

[45] J. Scheuer and M. Orenstein. Optical vortices crystals: Spontaneous generation in nonlinear semiconductor microcavities. *Science*, 230, 1999.

[46] C. Schindler and R. Zimmermann. Analysis of the exciton-exciton interaction in semiconductor quantum wells. *Phys. Rev. B*, 78:045313, 2008.

[47] G. J. Schinner, J. Repp, E. Schubert, A. K. Rai, D. Reuter, A. D. Wieck, A. O. Govorov, A. W. Holleitner, and J. P. Kotthaus. Confinement and interaction of single indirect excitons in a voltage-controlled trap formed inside double in gaas quantum wells. *Phys Rev. Lett.*, 110:127403, 2013.

[48] G. J. Schinner, J. Repp, E. Schubert, A. K. Rai, D. Reuter, A. D. Wieck, A. O. Govorov, A. W. Holleitner, and J. P. Kotthaus. Many-body correlations of electrostatically trapped dipolar excitons. *Phys Rev. B*, 87:205302, 2013.

[49] G. J. Schinner, E. Schubert, M. P. Stallhofer, J. P. Kotthaus, D. Schuh, A. K. Rai, D. Reuter, A. D. Wieck, and A. O. Govorov. Electrostatically trapping indirect excitons in coupled inxga1-xas quantum wells. *Phys Rev. B*, 83:165308, 2011.

[50] V. Schweikhard, I. Coddington, P. Engels, V. P. Mogendorff, and E. A. Cornell. Rapidly rotating bose-einstein condensates in and near the lowest landau level. *Phys. Rev. Lett.*, 92:040404, 2004.

[51] Y. Shilo, K. Cohen, B. Laikhtman, K. West, L. Pfeiffer, and R. Rapaport. Particle correlations and evidence for dark state condensation in a cold dipolar exciton fluid. *Nature Commun.*, 4:2335, 2013.

[52] G. E. Smith. Nobel lecture: The invention and early history of the ccd. *Rev. Mod. Phys*, 82:2307, 2010.

[53] A. Violante, K. Cohen, S. Lazic, R. Hey, R. Rapaport, and P. V. Santos. Dynamics of indirect exciton transport by moving acoustic fields. *New J. of Phys.*, 33035, 2014.

[54] X. P. Vogele, D. Schuh, W. Wegscheider, J. P. Kotthaus, and A. W. Holleitner. Density enhanced diffusion of dipolar excitons within a one-dimensional channel. *Phys. Rev. Lett.*, 103:126402, 2009.

[55] A. G. Winbow, J. R. Leonard, M. Remeika, Y. Y. Kuznetsova, A. A. High, A. T. Hammack, L. V. Butov, J. Wilkes, A. A. Guenther, A. L. Ivanov, M. Hanson, and A. C. Gossard. Electrostatic conveyer for excitons. *Phys. Rev. Lett.*, 106:196806, 2011.

[56] S. Zimmermann, A.O. Govorov, W. Hansen, J.P. Kotthaus, M. Bichler, and W. Wegscheider. Lateral superlattices as voltage-controlled traps for excitons. *Phys. Rev. B*, 56:13414–13421, 1997.

[57] S. Zimmermann, G. Schedelbeck, A. O. Govorov, A. Wixforth, J. P. Kotthaus, M. Bichler, W. Wegscheider, and G. Abstreiter. Spatially resolved exciton trapping in a voltage-controlled lateral superlattice. *Appl Phys. Lett.*, 73:154, 1998.